

EUMETSAT Satellite Application Facility on Climate Monitoring

The EUMETSAT
Network of
Satellite Application
Facilities



Algorithm Theoretical Baseline Document **Meteosat (M VIRI) Solar Surface Irradiance and effective Cloud Albedo Climate Data Sets**

The MAGICSOL method

CM SAF product identifier:

Surface Incoming Shortwave Radiation (SIS):	CM-54
Direct Irradiance at Surface (SID):	CM-106
Effective Cloud Albedo (CAL):	CM-111

Reference Number:

SAF/CM/DWD/ATBDRI_HEL

Version:

1.1

Date:

25 January 2011

 Algorithm Theoretical Basis Document Meteosat (MVIRI) Climate Data Sets of SIS, SID and CAL: MVIRI_HEL	Doc.No.: SAF/CM/DWD/ATBD/MVIRI_HEL Issue: Date: 25.01.2011
--	---

Document Signature Table

	Name	Function	Signature	Date
Author	Richard Mueller Jörg Trentmann	CM SAF scientist		05/11/2010
Author	Reto Stöckli Rebekka Posselt	CM SAF scientist		25/01/2011
Editor	Rainer Hollmann	Science Coordinator		30/05/2011
Approval	Rainer Hollmann	Science Coordinator		30/05/2011
Release	Martin Werscheck	Project Manager		

Distribution List

Internal Distribution	
Name	No. Copies
DWD Archive	1
CM SAF Team	1

External Distribution		
Company	Name	No. Copies
PUBLIC		1

Document Change Record

Issue/ Revision	Date	DCN No.	Changed Pages/Paragraphs
1.0	05/11/2010	SAF/CM/DWD/ATBD/MVIRI_HEL	First official version.
1.1	25.01.2011	SAF/CM/DWD/PUM/MVIRI_HEL	Modifications implemented according to the Review comments (minutes).

 Algorithm Theoretical Basis Document Meteosat (MVIRI) Climate Data Sets of SIS, SID and CAL: MVIRI_HEL	Doc.No.: SAF/CM/DWD/ATBD/MVIRI_HEL Issue: Date: 1.1 25.01.2011
--	---

Table of Contents

1 THE EUMETSAT SAF ON CLIMATE MONITORING (CMSAF)	7
1.1 Applicable Documents	8
1.2 Reference Documents	8
2 INTRODUCTION	8
3 THE MAGICSOL METHOD	10
3.1 The original Heliosat algorithm	10
3.2 From Heliosat to MAGICSOL	11
3.2.1 Self calibration	11
3.2.2 Clear sky reflection	13
3.3 Effective cloud albedo (CM-111, CAL)	15
3.3.1 Introduction	15
3.3.2 Averaging	15
3.3.3 Input data	15
3.4 Sensitivity of the effective cloud albedo on ρ_{\max} and ρ_{srf}	15
3.4.1 Sensitivity of CAL on self-calibration method	15
3.4.2 Sensitivity of CAL on clear sky reflection	16
3.5 Limitations, assumptions and future improvements	18
3.6 Relation of effective cloud albedo to solar irradiance	19
4 THE GNU-MAGIC ALGORITHM	20
4.1 Solar irradiance: Introduction and Definition	20
4.2 Motivation and strategy for solar surface irradiance and direct irradiance	20
4.3 Algorithm Overview	21
4.4 The GNU-MAGIC approach for the retrieval of solar irradiance	22
4.5 Atmospheric input information	23
5 SOLAR SURFACE IRRADIANCE (CM-54)	24
5.1 Cloudy sky situations	26
5.2 Averaging	26
5.3 Sensitivity and dependence of atmospheric input on SIS	27
5.3.1 Water vapour:	27
5.3.2 Ozone	28

 Algorithm Theoretical Basis Document Meteosat (MVIRI) Climate Data Sets of SIS, SID and CAL: MVIRI_HEL	Doc.No.: SAF/CM/DWD/ATBD/MVIRI_HEL Issue: Date: 25.01.2011
--	---

5.3.3	Aerosols	29
5.3.4	Surface albedo	31
5.3.5	Clear sky index	31
5.4	Assumption, limitations and future improvements	32
6	DIRECT IRRADIANCE (CM-106)	33
6.1	Averaging	34
6.2	Averaging	34
6.3	Sensitivity and dependence of atmospheric input on direct irradiance	34
6.3.1	Water vapour:	34
6.3.2	Ozone	35
6.3.3	Aerosols	36
6.3.4	Clear sky index	38
6.4	Assumption, limitations and future improvements	38
7	REFERENCES	39
8	GLOSSARY	41
9	APPENDIX A: GNU-MAGIC DOCUMENTATION CONTAINING FURTHER ALGORITHM INFORMATION OF GNU-MAGIC	41

 Algorithm Theoretical Basis Document Meteosat (MVIRI) Climate Data Sets of SIS, SID and CAL: MVIRI_HEL	Doc.No.: SAF/CM/DWD/ATBD/MVIRI_HEL Issue: Date: 1.1 25.01.2011
--	---

Table of Figures

Figure 3–1: Temporal evolution of the normalized differences between the CM SAF data set and the BSRN data including the trend coloured in red. The trend is not significant, both concerning the statistical significance and the magnitude. The absence of an trend in relation to the large trends in the digital satellite counts (Figure 3–2) demonstrates that the self-calibration works well.	12
Figure 3–2: Time series of ρ_{\max} from 1983 to 2006. The different colours are assigned to the different Meteosat satellites M2_M7 as given in the legend.	13
Figure 3–3: Sensitivity of the effective cloud albedo on the ρ_{\max} uncertainty for different surface types, with an albedo of 0.05 (~ocean), 0.15 (~vegetation) and 0.35 (~desert).	16
Figure 3–4: Sensitivity of the effective cloud albedo on the clear sky reflection ρ_{srf} . The x-axis compiles the range of the cloud index. On the y-axis the uncertainty or error of the effective cloud albedo is given for different surface types and uncertainties in the retrieval of ρ_{srf} of 2% and 4%, respectively, arising from “statistical noise”. The effect of uncertainties of ρ_{srf} on the effective cloud albedo is rather weak. Only for desert (sand) surface an errors in the retrieval of ρ_{srf} would lead to significant errors in the effective cloud albedo.	17
Figure 3–5: Effect of cloud contamination of clear sky reflection on the effective cloud albedo. The effect is rather large. However it occurs pre-dominantly at the border region of the MFG disk. Further on, the effect occurs for long-lasting cloud coverage, the resulting higher uncertainty in the effective cloud albedo has therefore a relative small effect on SIS.	17
Figure 3–6: Examples of ρ_{sfc} images, here for 2000, 12 GMT, from top left to bottom right, December, March, June and September. The white speckle patterns beyond the white lines close to the border of the disk are due to significant cloud contamination of ρ_{sfc} . However, close to the poles, some white regions are not an artefact but due to ice (Greenland & Arctic in the September image). Cloud contamination occurs also in a small band around sunrise and sunset at the East and West border of the disk, respectively. However, the core of the Meteosat disk is almost not affected.	18
Figure 4–1: Principle of solar-thermal power plants: The concentration of solar surface irradiance enables the generation of high temperatures, hence the operation of “traditional” cost-efficient steam generators. Various prototypes have already been set up in southern Europe and Morocco.	20
Figure 4–2: The relation of the transmission to a manifold of atmospheric states is pre-calculated with a radiative transfer model (RTM) and saved in a look-up table (LUT). Once, the LUT has been computed the transmittance for a given atmospheric state can be extracted from the LUT for each satellite pixel and time.	21
Figure 4–3: Diagram of the interface of MAGIC to the atmospheric input and the satellite observations, C_{eff} stands for the dark offset corrected and normalised Counts.	23
Figure 5–1: Flow-diagram of the clear sky LUT approach for SIS. NWP: Numerical Weather Prediction.	25
Figure 5–2: The sensitivity of solar surface SIS irradiance on water vapour variations for a SZA of 0° and 60°.	27
Figure 5–3: The sensitivity of “total” solar irradiance in relation to that of direct irradiance at an air mass of 2 (SZA=60°). As can be seen the effect is not very large as both quantities show almost the same sensitivity.	28
Figure 5–4: The sensitivity of solar irradiance SIS to ozone for a SZA of 0° and 60°.	29
Figure 5–5: Sensitivity of Aerosol optical depth and single scattering albedo on direct irradiance in comparison to total solar irradiance for a solar zenith angle of 60° (air mass of 2).	30
Figure 5–6: Sensitivity of Aerosol optical depth and single scattering albedo on direct irradiance in comparison to total solar irradiance for a solar zenith angle of 0°. (air mass of 2).	30
Figure 5–7: Sensitivity of the solar irradiance SIS on the surface albedo. The red line shows the RTM results and the green line the applied parameterisation. The horizontal axis shows the deviation of SIS with variable surface albedo relative to SIS calculated for a fixed surface albedo of 0.2. For deviations of +/- 0.1 in the surface albedo the uncertainty in SIS is +/- 1%. With exception of values above 0.9 the parameterisation matches the RTM results well.	31
Figure 6–1: Flow-diagram of the clear sky LUT approach. NWP: Numerical Weather Prediction.	33

 Algorithm Theoretical Basis Document Meteosat (MVIRI) Climate Data Sets of SIS, SID and CAL: MVIRI_HEL	Doc.No.: SAF/CM/DWD/ATBD/MVIRI_HEL Issue: 25.01.2011 1.1 Date:
--	---

Figure 6–2: The sensitivity of direct irradiance on water vapour for a SZA of zero and 60 degree.....	35
Figure 6–3: The sensitivity of direct irradiance to ozone for a SZA of zero and 60 degree.	36
Figure 6–4: Sensitivity of Aerosol optical depth and single scattering albedo on direct irradiance in comparison to total solar irradiance for a solar zenith angle of 60 degree (air mass of 2)	37
Figure 6–5: Sensitivity of Aerosol optical depth and single scattering albedo on direct irradiance in comparison to total solar irradiance for a solar zenith angle of 0 degree.	37
Figure 6–6: Sensitivity of direct irradiance on the clear sky index.	38

 CM SAF Climate Monitoring	Algorithm Theoretical Basis Document Meteosat (MVIRI) Climate Data Sets of SIS, SID and CAL: MVIRI_HEL	Doc.No.: SAF/CM/DWD/ATBD/MVIRI_HEL Issue: Date: 25.01.2011
--	---	---

1 The EUMETSAT SAF on Climate Monitoring (CMSAF)

EUMETSAT has started the development of a Network of Satellite Application Facilities (SAF) which together with the EUMETSAT central facilities constitute the EUMETSAT Application Ground Segments for MSG and EPS. The SAFs are located in a National Meteorological Service or other approved institutes of a EUMETSAT member state. The scope of the SAF activities is to deliver products, at the level of geophysical parameters, based primarily on the satellite data.

The Satellite Application Facility on Climate Monitoring (CM SAF) targeted its development in the period 1999-2003 on generation and archiving high quality data sets on a continuous basis for the analysis and monitoring of the climate system, its changes and the validation of numerical models (climate and NWP models). The CM SAF started an Initial Operations Phase (IOP) covering the period January 2004 to February 2007. The objectives of the CMSAF IOP were mainly the operational production, control and distribution of products developed in the previous phase, and to carry out research and development for an extension of the product line with new sensors and platforms. The Continuous Development and Operations Phase (CDOP) started in 2007 covering the period March 2007 – February 2012. This CDOP covers – among others – the continuation and further development of the products from the IOP, addition of further GCOS ECV's, but also the provision of long-term data sets with known error characteristics and temporal stability.

The consortium of CM SAF currently comprises the Deutscher Wetterdienst (DWD) as host institute, and the partners from the Royal Meteorological Institute of Belgium (RMIB), the Finnish Meteorological Institute (FMI), the Royal Meteorological Institute of the Netherlands (KNMI), the Swedish Meteorological and Hydrological Institute (SMHI) and the Meteorological Service of Switzerland (MeteoSwiss).

CM SAF data products are distinguished in operational monitoring products and retrospectively produced data sets (Schulz et al. (2009)). Operational monitoring products are disseminated with high timeliness (within 8 weeks after observation) to support operational climate monitoring application of National Meteorological and Hydrological Services. The timeliness requirement most likely makes this type of product not suitable for monitoring of inter-annual variability and trends with high confidence. Bias errors due to shift of equator overpass times and orbit height decay as well as instrument caused inter-satellite biases are not corrected for in the operational monitoring product. However, the characterisation of relatively strong anomalies on monthly scale should be possible.

Within the retrospectively produced data sets the above described errors are minimised to level that the data sets can safely be used to analyse variability at longer scales than inter-annual. CM SAF aims at the delivery of such data sets for a number of ECVs, as defined by GCOS.

A catalogue of available CM SAF products is available via the CM SAF webpage <http://www.cmsaf.eu/>. Here, detailed information about product ordering, add-on tools, sample programs and documentation are provided.

 CM SAF Climate Monitoring	Algorithm Theoretical Basis Document Meteosat (MVIRI) Climate Data Sets of SIS, SID and CAL: MVIRI_HEL	Doc.No.: SAF/CM/DWD/ATBD/MVIRI_HEL Issue: 1.1 Date: 25.01.2011
--	---	---

1.1 Applicable Documents

Reference	Title	Code
AD 1	CM SAF Product Requirements Document	SAF/CM/DWD/PRD/1.6

1.2 Reference Documents

Reference	Title	Code
RD.1	Validation Report Meteosat (MVIRI) Climate Data Set of SIS, SID and CAL : MVIRI_HEL	SAF/CM/DWD/VAL/MVIRI_HEL/1.0
RD.2	Product User Manual Meteosat (MVIRI) Climate Data Set of SIS, SID and CAL : MVIRI_HEL	SAF/CM/DWD/PUM/MVIRI_HEL/1.0

2 Introduction

Long time series are needed for climate monitoring and analysis. For this reason there is a need to employ the satellite information of the first generation of Meteosat satellites (Meteosat-2 to Meteosat-7) to generate climate information. The MVIRI instrument onboard the Meteosat First Generation satellite is equipped with 3 channels: a broadband channel in the visible, a channel in the Infrared, and a water vapour channel.

The second generation of Meteosat satellites is equipped with the Spinning Enhanced Visible and InfraRed Imager (SEVIRI) and the Geostationary Earth Radiation Budget (GERB) instrument. The GERB instrument is a visible-infrared radiometer for earth radiation budget studies. It provides accurate measurements of the shortwave (SW) and longwave (LW) components of the radiation budget at the top of the atmosphere. SEVIRI employs twelve spectral channels, which provide more information of the atmosphere compared to its forerunner. Several retrieval algorithms have been developed in order to use the additional information gained by the improved spectral information of MSG mainly for now-casting applications. However, these algorithms can not be applied to the MVIRI instrument onboard the Meteosat First Generation satellites as they use spectral information that is not provided by MFG (NWC SAF cloud algorithm, CM SAF radiation algorithm).

MVIRI is a passive imaging radiometer with three spectral channels: a visible channel covering 500-900 nm, and infra-red channel covering 5.7-7.1 microns and 10.5-12.5 microns. MVIRI comes with a spatial resolution of 2.5km for the visible and 5km for the IR channels, sub-satellite point respectively.

Hence, in order to be able to provide a long time series covering more than 20 years there is a need for a specific climate algorithm that can be applied to the satellites from the Meteosat First and Second Generation. Moreover, the retrieved climate variable must have climate quality.

The MAGICSOL method in combination with the gnu-public license version of MAGIC does meet the above mentioned requirements. The method provides the effective cloud albedo, the solar surface irradiance, and the net shortwave radiation, i.e., all components of the GCOS Essential Climate Variables (ECVs) surface radiation budget and cloud properties.

The applied Heliosat method needs only the broadband visible channel as satellite information and can therefore be applied to MFG and across different satellite generations.

 Algorithm Theoretical Basis Document Meteosat (MVIRI) Climate Data Sets of SIS, SID and CAL: MVIRI_HEL	Doc.No.: SAF/CM/DWD/ATBD/MVIRI_HEL Issue: Date: 25.01.2011
--	---

The application to other geostationary satellites, e.g., in the US and Asia is also possible. Hence, the Heliosat method has not only the power to provide long time series of ECVS, but also to provide ECVs, which cover the complete geostationary ring.

The Heliosat method, which is well established in the solar energy community, is the basis of the MAGICSOL method for clouds. However, modifications of the original Heliosat method are needed to meet the requirements to generate a Climate Data Record.

Table 2-1: Overview of MVIRI based data sets retrieved with MAGICSOL and discussed in this ATBD.

Acronym	Product title	Unit
SIS	Surface Incoming Shortwave Irradiance	W m^{-2}
CAL	Effective Cloud Albedo	Dimensionless
SID	Direct Irradiance at surface	W m^{-2}

 Algorithm Theoretical Basis Document Meteosat (MVIRI) Climate Data Sets of SIS, SID and CAL: MVIRI_HEL	Doc.No.: SAF/CM/DWD/ATBD/MVIRI_HEL Issue: Date: 25.01.2011
--	---

3 The MAGICSOL method

3.1 The original Heliosat algorithm

The Heliosat algorithm uses reflection measurements given as normalized digital counts to determine the effective cloud albedo, also called cloud index (Cano et al., 1986; Beyer et al., 1996; Hammer et al., 2003). A clear sky model is used to calculate the solar surface irradiance based on the retrieved effective cloud albedo.

Basis of the Heliosat method are the rectified digital pixel counts of a visible Meteosat channel (High Resolution Visible). The respective data are called “*Rectified Image Data*” and provided by EUMETSAT (EUM TD 06). No information from other channels is used. The first step in the Heliosat method is the retrieval of the effective cloud albedo (cloud index). The effective cloud albedo is defined as the normalised relation between the all sky and clear sky reflection in the visible observed by the satellite. The deviation of the actual reflection of the pixel from the clear sky reflection is a measure of the cloudiness. The brighter the pixel the more or thicker clouds are present. Thereby, the changes in the reflective properties of the clouds due to different insulation angles during the day and year are accounted for by a normalization with the sun elevation ($\cos(\Theta_z)$ - cosine of the sun's zenith angle) and a correction for the sun-earth distance f . Furthermore, the measured count value D is reduced by the dark offset D_0 , which is a satellite specific value obtained by looking into dark space. Values below the dark offset are, thus, assumed to be zero.

$$\text{Equation 3.1: } \rho = \frac{D - D_0}{f \cos(\Theta_z)}$$

Here, D is the observed digital count including the dark offset of the satellite instrument. The dark offset does not arise from the Earth reflection but is an intrinsic instrument offset and has therefore to be subtracted. The effect of the sun-earth distance is considered by the factor f , finally, the cosine of the solar zenith angle corrects the different illumination conditions at the top of atmosphere introduced by different solar altitudes.

The effective cloud albedo is then derived from the normalized pixel count ρ , the clear sky reflection ρ_{srf} and the albedo of a compact (not convective) cloud deck ρ_{max} by

$$\text{Equation 3.2: } n = \frac{\rho - \rho_{srf}}{\rho_{max} - \rho_{srf}}$$

Here, ρ is the observed reflection for each pixel and time. ρ_{srf} is the clear sky reflection, which is a monthly value determined for every pixel separately. In principle this is done by using the reflection of the pixel in a cloud free case. This is usually the lowest occurring reflection during a certain time span (e.g., a month) derived for each pixel of the satellite image. ρ_{max} is the “maximum” cloud albedo. It could be determined in a similar fashion by choosing the “maximum” ρ per pixel and time span (Beyer et al., 1996) or by using a single value for the full disk that is dependent on the radiometer of the different satellites (Hammer et al., 2003). MAGICSOL follows the approach of Hammer et al. (2003) but a target region is used instead of the whole disk. One value of ρ_{max} is retrieved for each month, please see section 3.2.1 for further details.

 Algorithm Theoretical Basis Document Meteosat (MVIRI) Climate Data Sets of SIS, SID and CAL: MVIRI_HEL	Doc.No.: SAF/CM/DWD/ATBD/MVIRI_HEL Issue: Date: 25.01.2011
--	---

3.2 From Heliosat to MAGICSOL

To meet the requirements of CDR processing modifications on the original Heliosat algorithm have been performed, leading to a Climate specific version of Heliosat. The modified version in combination with the gnu-MAGIC approach is called MAGICSOL.

3.2.1 Self calibration

The self-calibration algorithm is based on an operational determination of the “maximum” effective cloud albedo ρ_{\max} . Input are sun zenith angle normalised counts corresponding to Equation 3.1

In analogy to Rigollier et al. (2002) a histogram of all available counts is generated. However, instead of using an upper and a lower bound, only the 95%-percentile is used as self-calibration parameter and set to ρ_{\max} (Hammer et al, 2003 and references therein).

However, the generation of the histogram for the full disk is rather slow due to the large pixel amount. Thus, a reduction of the considered region for the histogram was necessary. The selected region is located in the southern ocean between 15° W and 0° W and 58° S and 48° S. It features a high abundance of frontal systems with large cloud amounts most of the time, but hardly any convection.

A range of percentiles has been tested and the 95 percentile has been found to provide the best statistical stability. Using a percentile value and not the maximum of the histogram should exclude saturated pixels, which may have technical but no scientific reasons, and it also should exclude potential convective clouds. Depending on the applied method deep convective clouds might be useful for calibration, but they affect the stability of the 95 percentile applied within the MAGICSOL method

The self-calibration algorithm is run at the 13 o'clock slot GMT which accounts for the slight westward shift of the region. The histogram is generated with a month worth of satellite data input. The resulting ρ_{\max} is then applied for all slots within that month.

Figure 3–1 shows the temporal evolution of the normalized bias between the CM SAF data set and the BSRN data. The normalized difference is calculated as follows:

The arithmetic average over the complete time series of the BSRN and the satellite data is calculated for each station. The resulting mean difference (bias) is subtracted from all monthly means of the satellite data for each station. The mean difference (bias) over the covered time period is zero afterwards; however, **trends in the monthly differences are not affected by this normalization procedure**.

The differences between the monthly means of BSRN and satellite data are then averaged over all available stations, whenever monthly means from at least 3 stations are available. This leads to an overall time series of “normalized” differences of monthly means. This time series is then analysed for temporal trends. A trend in this time series would indicate inhomogeneities introduced by the self-calibration or the clear sky reflection maps. The applied method is necessary in order to avoid misleading trends in the monthly differences introduced by the different start and end points of the time series and the corresponding mismatch in the weighting of regional bias values. For the test of the self-calibration it is necessary to avoid artefacts due to local bias values as only the temporal evolution of the time series for the complete disk is of relevance. Contrary, the temporal evolution of the normalised mean monthly differences is not affected by the different numbers of available stations for certain months and their local bias:

As can be seen there is no detectable trend in the temporal evolution of the normalized monthly differences, which proves evidence of the homogeneity of the SIS time series. In contrast, the satellite raw counts show a significant and large trend, a decrease of the sensibility due to aging, see Figure 3–2. The absence of this trend in the normalized differences of the SIS data demonstrates the ability of the self-calibration method to correct for aging and satellite switches.

 Algorithm Theoretical Basis Document Meteosat (MVIRI) Climate Data Sets of SIS, SID and CAL: MVIRI_HEL	Doc.No.: SAF/CM/DWD/ATBD/MVIRI_HEL Issue: Date: 1.1 25.01.2011
--	---

It is worth noting that a statistically significant negative trend in the normalized differences is present in the GEWEX and ISCCP SIS data sets

Because the Heliosat method is dedicated to retrieve the effective cloud albedo, a "clear sky" surface target has been not implemented for the self-calibration. Using a land surface target would introduce errors in the self-calibration method as the aging detected by observation of surface reflection is different to that detected with an appropriate cloud target. This is due to the stronger aging of optical devices in the UV and UV-near spectral regions, which leads to different rates of aging for the various land surface types (due to different spectral responses of the targets) in relation to clouds. Every aging of "clear sky" reflection for the different surface types are automatically considered by the retrieval of the planetary clear sky reflection ρ_{sr} (see section 3.2.2).

Temporal evolution of normalized differences

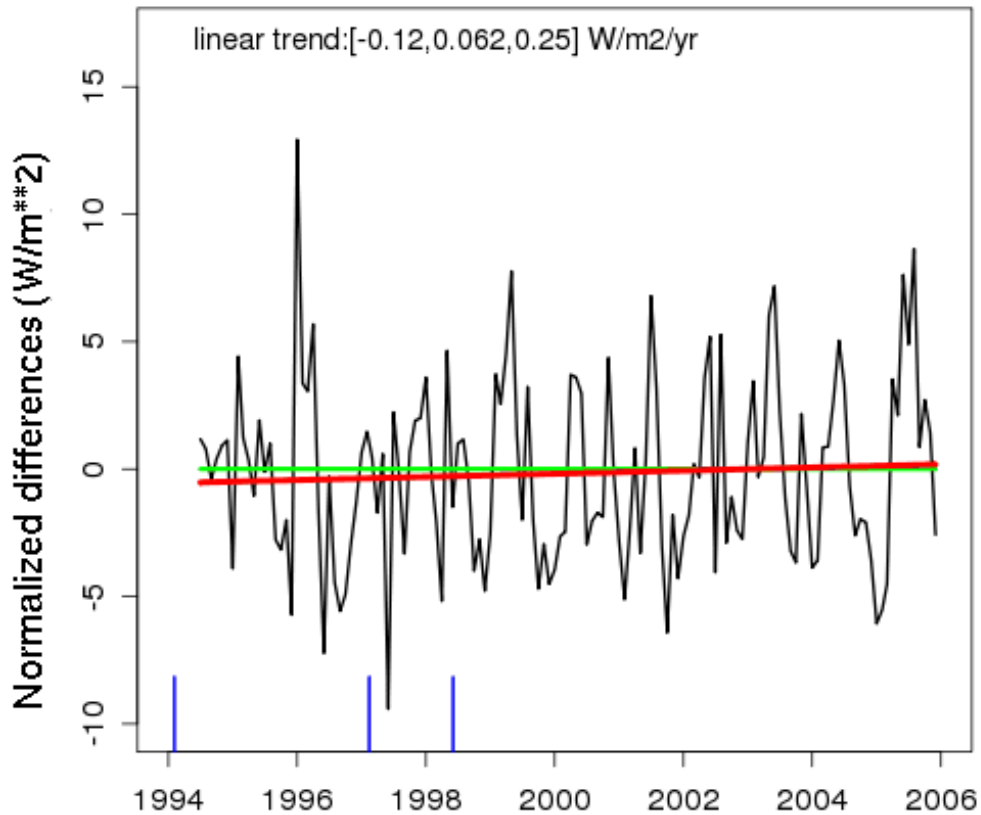


Figure 3–1: Temporal evolution of the normalized differences between the CM SAF data set and the BSRN data including the trend coloured in red. The trend is not significant, both concerning the statistical significance and the magnitude. The absence of a trend in relation to the large trends in the digital satellite counts (Figure 3–2) demonstrates that the self-calibration works well.

 Algorithm Theoretical Basis Document Meteosat (MVIRI) Climate Data Sets of SIS, SID and CAL: MVIRI_HEL	Doc.No.: SAF/CM/DWD/ATBD/MVIRI_HEL Issue: Date: 1.1 25.01.2011
--	---

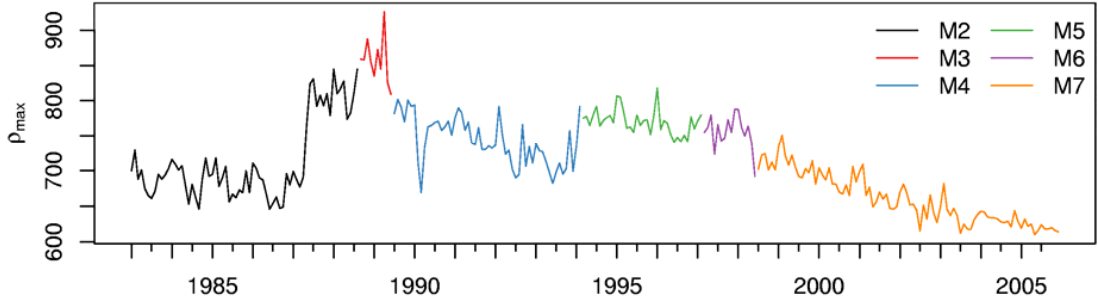


Figure 3–2: Time series of ρ_{\max} from 1983 to 2006. The different colours are assigned to the different Meteosat satellites M2_M7 as given in the legend.

Meteosat-1 data quality is too worse to be used for the data set. The jump around 1987 within the M2 time series is due to a gauge change of the instrument, performed by the EUMETSAT ground segment. The gauge jump has been well detected and corrected by the self-calibration method as well as the large instrument degradation given for Meteosat-7 (see validation report).

3.2.2 Clear sky reflection

The processing of the long time series of global radiation from Meteosat's first generation satellites employs a newly implemented clear sky or background reflection algorithm for Heliosat (Duerr and Zelenka, 2009). Instead of having a monthly constant field of the clear sky reflection ρ_{srf} , a seven day running mean reflection field is used. Thus, sudden changes in the clear sky reflection due to, e.g., vegetation and snow are captured and represented faster than with the standard method. In addition, sudden jumps in the cloud index at month borders due to larger differences in the clear sky reflection fields are avoided.

The selection of a 7 day running mean is based on the publication by Zelenka (1999) where this time series approach has been introduced. It is justified with the persistence of weather patterns in the order of 5 to 7 days. However, problems with longer lasting overcast episodes phenomena as e.g. fog can occur and might lead errors in the cloud index retrieval.

The presented clear sky reflection algorithm is also able to detect snow and, thus, gives the opportunity to correct for some of the radiative properties of snow. The clear sky reflection is dominated by the surface reflection.

The algorithm to determine the clear sky reflection ρ_{srf} is based on two tests that are applied to the TOA apparent reflection (ρ) in order to determine the evolution of ρ_{srf} . If both tests fail, i.e. if ρ is rather large as occurring in case of clouds and snow, ρ_{srf} is not changed.

 Algorithm Theoretical Basis Document Meteosat (MVIRI) Climate Data Sets of SIS, SID and CAL: MVIRI_HEL	Doc.No.: SAF/CM/DWD/ATBD/MVIRI_HEL Issue: Date: 1.1 25.01.2011
--	---

$$\text{Test 1: } (\rho \leq \rho_{srf} + \varepsilon_{up} \& \rho > \rho_{srf}) \mid (\rho < \rho_{srf} - \varepsilon_{low}) \rightarrow \rho_{srf} = \frac{6}{7} \rho_{srf} + \frac{1}{7} \rho$$

(slow evolution)

$$\text{Test 2: } (\rho < \rho_{srf} \& \rho \geq \rho_{srf} - \varepsilon_{low}) \rightarrow \rho_{srf} = \frac{1}{2} \rho_{srf} + \frac{1}{2} \rho$$

(fast evolution)

$$\text{else: } \rightarrow \rho_{srf} = \rho_{srf}$$

(no change)

In contrast to Zelenka (2001), variable bandwidths ε_{up} and ε_{low} are employed (Equation 3.1), which were presented by Duerr and Zelenka (2009) with ρ_{max} being the satellite calibration constant, see section 3.2.1.

Equation 3.3:

$$\varepsilon_{up} = 0.125 \rho_{max} + \frac{8(\rho_{srf} - 0.15 \rho_{max})}{0.25 \rho_{max}}$$

$$\varepsilon_{low} = 0.0875 \rho_{max} + \frac{6(\rho_{srf} - 0.15 \rho_{max})}{0.25 \rho_{max}}$$

If Test 1 and Test 2 fail for a certain number of days (i.e., a very bright pixel all the time) then this pixel is assigned to be snow covered. The presented time-series approach is based on the very low temporal variability of snow compared to clouds. Thus, continuously detecting very high reflectivity's in one time slot over a certain number of days indicate snow. Problems occur in cases of persistent fog or cloud decks (e.g., marine stratocumulus). In case of a positive snow detection the clear sky reflection is adapted as fast evolution.

The threshold number of days for the snow detection is set to 24. This amount is reduced to 6 in case the considered pixel already had a snow event. This is given by either an amplitude $\rho_{srf} = \rho_{srf,max} - \rho_{srf,min}$ exceeding $0.55 \rho_{max}$ or by ρ being larger than a snow threshold ρ_{snow} . The latter is derived empirically so that it is high enough to exclude oceans or other dark surfaces ($\rho_{snow,min}$) and that it favors pixels that have a high ρ_{srf} and thus a higher probability of a former snow event ($\rho_{snow,range}$), see Equation 3.4.

Equation 3.4:

$$\rho_{snow,min} = 0.48 \rho_{max}$$

$$\rho_{snow,range} = \max(0.15 \rho_{max}, 0.6 \rho_{srf,max})$$

$$\rho_{snow} = \max(\rho_{snow,min}, \rho_{srf,min} + \rho_{snow,range})$$

The calculation of the cloud index n for non-snow pixels follows the standard Heliosat. In case snow is detected the calculation of the cloud index n is altered according to Duerr and Zelenka (2009) in which ρ_{srf} is substituted by $\rho_{snow,min}$ and ρ_{max} is increased by a factor of 1.41 in order to enhance the dynamic range (Equation 3.5). This altered cloud index formulation generally gives lower cloud index values in order to account for the radiative properties of snow. This includes mainly the reflectivity of the bright snow surface which leads to higher surface radiation values.

 Algorithm Theoretical Basis Document Meteosat (MVIRI) Climate Data Sets of SIS, SID and CAL: MVIRI_HEL	Doc.No.: SAF/CM/DWD/ATBD/MVIRI_HEL Issue: Date: 25.01.2011
--	---

Equation 3.5:
$$n = \frac{\rho - 0.48\rho_{\max}}{1.41\rho_{\max} - 0.48\rho_{\max}} = \frac{\rho - 0.48\rho_{\max}}{0.93\rho_{\max}}$$

3.3 Effective cloud albedo (CM-111, CAL)

3.3.1 Introduction

The effective cloud albedo is derived with the MAGICSOL method described in section 3. Clouds have a net cooling effect, which is several magnitudes higher than the forcing cause by the increase of greenhouse gases. Every trend and anomalies in the effective cloud albedo would significantly effect the climate system on a global and/or regional scale. The effective cloud albedo is therefore an essential climate variable. As clouds can be assumed as Lambertian surfaces, the derived quantity can be considered the effective cloud albedo.

3.3.2 Averaging

Monthly, daily and hourly means are calculated by arithmetic averaging, using Equation 3.6 .

Equation 3.6:
$$\text{CAL}_{\text{mean}} = \frac{\sum_{i=1}^n \text{CAL}_i}{n}$$

Here i is a loop over the slots per hour for the calculation of hourly means, a loop over the hourly means for the calculation of the daily means and a loop over daily means for the calculation of monthly means. The conversion from the irregular satellite projection to the regular 0.03x0.03 degree grid is done with IDL using triangulation regridding (TRIGRID).

CALi is either the i-th daily mean for the calculation of the monthly mean or the i-th hourly mean for the calculation of the daily means. Only the finite values of CAL are summed up, n is the total number of finite values

3.3.3 Input data

MVIRI images of the broadband channel in openMTP format. However, other formats and satellite images can be treated as well.

3.4 Sensitivity of the effective cloud albedo on ρ_{\max} and ρ_{srf}

The effective cloud albedo is defined as a relative quantity of observed counts or radiances. Hence, any noise or uncertainty in the satellite observations is predominantly cancelled out. The uncertainty in the effective cloud albedo is therefore pre-dominantly determined by uncertainties in the determination of the clear sky reflection and the self-calibration method.

3.4.1 Sensitivity of CAL on self-calibration method

The uncertainty or fuzziness in ρ_{\max} defined by the month to month variations of ρ_{\max} is in the order of 3%. However, it is likely that part of this uncertainty is due to local biases in the

 Algorithm Theoretical Basis Document Meteosat (MVIRI) Climate Data Sets of SIS, SID and CAL: MVIRI_HEL	Doc.No.: SAF/CM/DWD/ATBD/MVIRI_HEL Issue: Date: 25.01.2011 1.1
--	--

satellite counts and not due to errors in the retrieval of ρ_{\max} . Local biases of the satellite counts would transfer to equal relative amounts into ρ_{\max} and ρ_{srf} , and would be therefore pre-dominantly cancelled out within the calculation of the effective cloud albedo (Equation 3.2). Hence, they would not affect the accuracy of CAL. However, as it is not possible to estimate to which amount the local biases counts to the ρ_{\max} uncertainty the complete uncertainty is assumed to arise from the applied statistical retrieval method. This is a worst case approach, since the uncertainty given by the ρ_{\max} retrieval method is likely significantly smaller than 3% and hence also the effect of the ρ_{\max} retrieval method on the accuracy of CAL. The ρ_{\max} uncertainty is constant in terms of relative uncertainty throughout the cloud index interval, but different for different surface types. Figure 3–3 shows the effect of a 3 % uncertainty on ρ_{\max} on the effective cloud albedo in absolute values. For a CAL value of 1 the absolute value is equal to the relative uncertainty, which is constant throughout the CAL range.

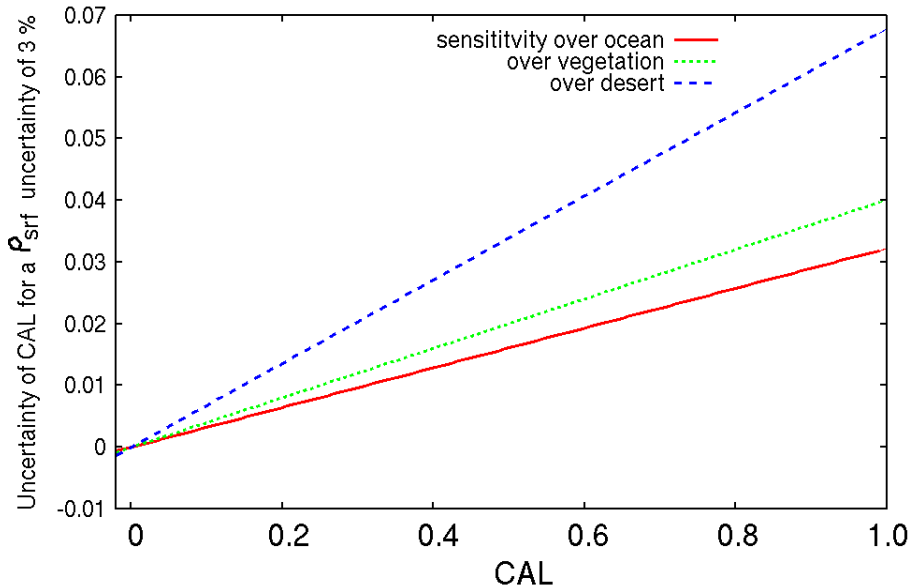


Figure 3–3: Sensitivity of the effective cloud albedo on the ρ_{\max} uncertainty for different surface types, with an albedo of 0.05 (~ocean), 0.15 (~vegetation) and 0.35 (~desert).

3.4.2 Sensitivity of CAL on clear sky reflection

Figure 3–4 shows the effect on uncertainties in the clear sky reflection on the effective cloud albedo. The effect is rather weak, as a consequence of the occurrence of ρ_{srf} in the dominator and nominator of the effective cloud albedo formula. However, the clear sky reflection introduces significant uncertainty and error in the effective cloud albedo retrieval for the case of cloud contamination. This happens if not enough clear sky cases occur. Hence, for regions with long-lasting cloud cover in combination with slant geometry the ρ_{srf} retrieval fails to see the clear sky situations, hence ρ_{srf} is contaminated by clouds and is artificially increased, see Figure 3–5. This effect occurs pre-dominantly at the border of the MFG disk,

 Algorithm Theoretical Basis Document Meteosat (MVIRI) Climate Data Sets of SIS, SID and CAL: MVIRI_HEL	Doc.No.: SAF/CM/DWD/ATBD/MVIRI_HEL Issue: Date: 1.1 25.01.2011
--	---

above 60 degrees, see Figure 3–6. As it occurs only for regions with long-lasting cloud coverage (hence large values of the effective cloud albedo) the effect on the solar irradiance is much lower as implied by the uncertainty in the effective cloud albedo.

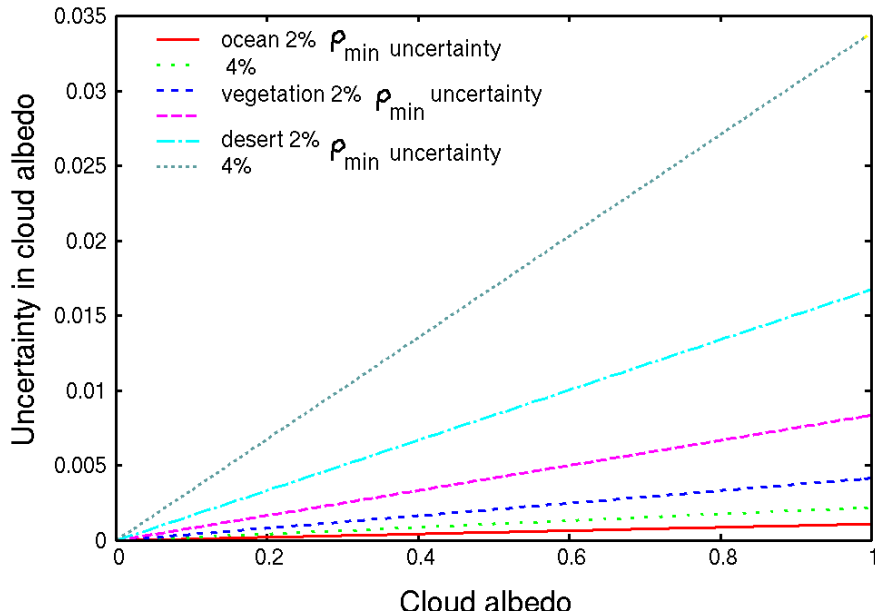


Figure 3–4: Sensitivity of the effective cloud albedo on the clear sky reflection ρ_{srf} . The x-axis compiles the range of the cloud index. On the y-axis the uncertainty or error of the effective cloud albedo is given for different surface types and uncertainties in the retrieval of ρ_{srf} of 2% and 4%, respectively, arising from “statistical noise”. The effect of uncertainties of ρ_{srf} on the effective cloud albedo is rather weak. Only for desert (sand) surface an errors in the retrieval of ρ_{srf} would lead to significant errors in the effective cloud albedo.

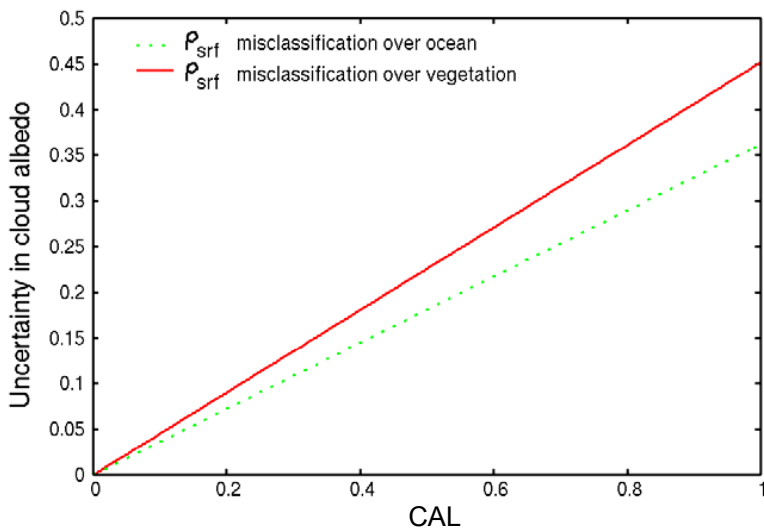


Figure 3–5: Effect of cloud contamination of clear sky reflection on the effective cloud albedo. The effect is rather large. However it occurs pre-dominantly at the border region of the MFG disk. Further on, the effect occurs for long-lasting cloud coverage, the resulting higher uncertainty in the effective cloud albedo has therefore a relative small effect on SIS.

 Algorithm Theoretical Basis Document Meteosat (MVIRI) Climate Data Sets of SIS, SID and CAL: MVIRI_HEL	Doc.No.: SAF/CM/DWD/ATBD/MVIRI_HEL Issue: Date: 25.01.2011
--	---

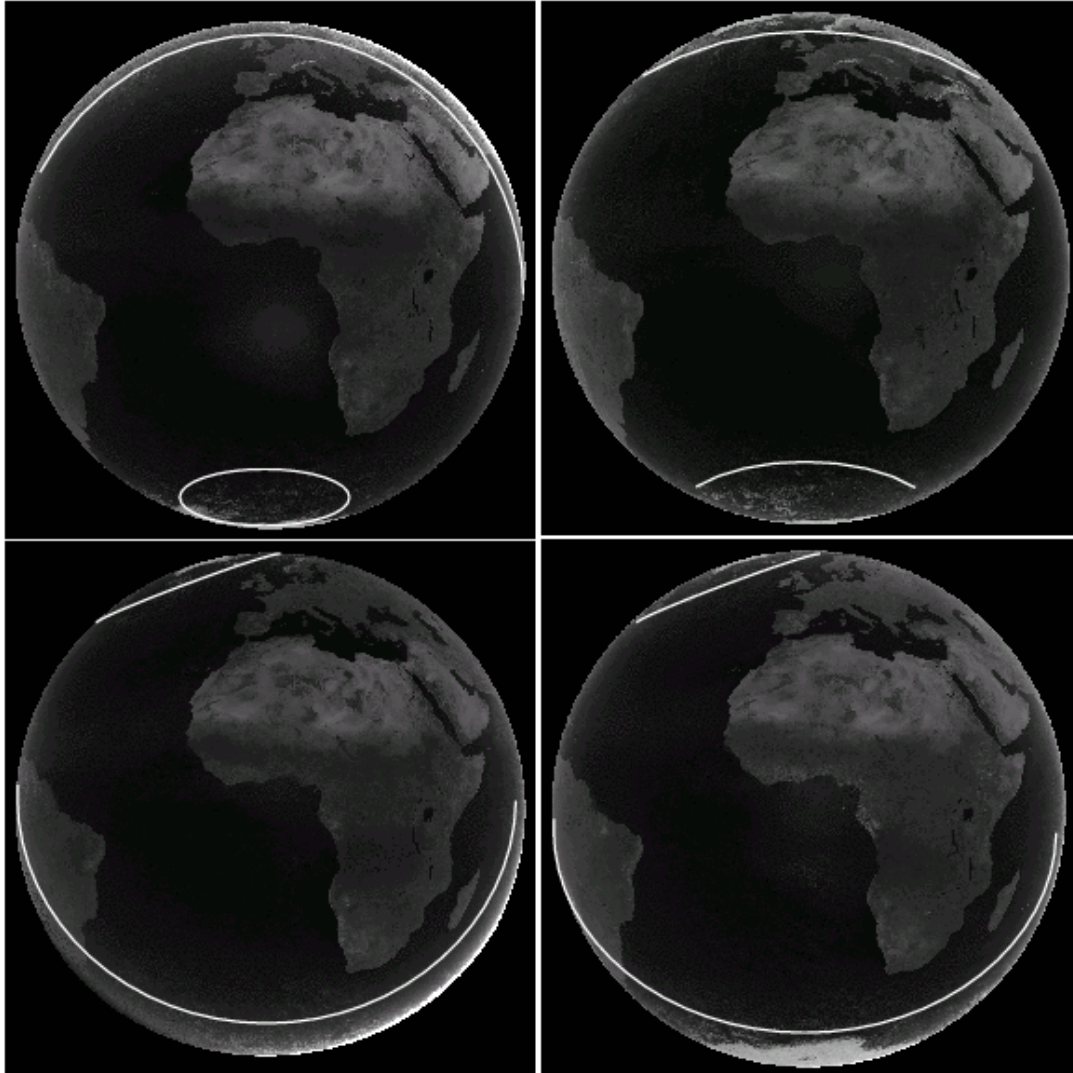


Figure 3–6: Examples of ρ_{sf} images, here for 2000, 12 GMT, from top left to bottom right, December, March, June and September. The white speckle patterns beyond the white lines close to the border of the disk are due to significant cloud contamination of ρ_{sf} . However, close to the poles, some white regions are not an artefact but due to ice (Greenland & Arctic in the September image). Cloud contamination occurs also in a small band around sunrise and sunset at the East and West border of the disk, respectively. However, the core of the Meteosat disk is almost not affected.

3.5 Limitations, assumptions and future improvements

Below is a list of some of known deficiencies and limitations of the CAL CDR:

- The above mentioned limitation is linked with the limitation related to the retrieval of ρ_{sf} , which can only be retrieved accurately if a certain amount of clear sky cases are given within a month. This is not always the case.

 Algorithm Theoretical Basis Document Meteosat (MVIRI) Climate Data Sets of SIS, SID and CAL: MVIRI_HEL	Doc.No.: SAF/CM/DWD/ATBD/MVIRI_HEL Issue: Date: 25.01.2011
--	---

- The anisotropy of the cloud reflection leads to uncertainties in the effective cloud albedo and subsequent in the solar surface irradiance. The respective effect is in the order of 1 to 2 % for monthly and daily means respectively. An improved correction of the anisotropy effect will be developed for the next release. However, in general the anisotropy effect is rather small.
- The self calibration method in combination with the modified retrieval of ρ_{srf} is sensible to significant changes in spectral channels. This implies that using the VIS006 or the VIS008 channel of MSG instead of the broadband channel will lead to significant differences in the effective cloud albedo in specific regions (please see Posselt et al, 2011 for further details). The item is not relevant for the discussed MVIRI climate data sets herein but for the planned prolongation of the record by the use of SEVIRI on board of MSG.

3.6 Relation of effective cloud albedo to solar irradiance

The effective cloud albedo is related to the solar irradiance via the clear sky index. The clear sky index, k, is defined as

$$k = SIS / SIS_{CLS}$$

Here SIS_{CLS} is the solar irradiance for cloud free skies. The relation between the effective cloud albedo CAL and the clear sky index is mainly given by:

$$k = 1 - CAL$$

This relation is defined by physics, in detail by the law of energy conservation (Dagedest, 2005). However, above a CAL value of 0.8 empirical corrections are needed, described in detail in section 5.1. With the knowledge of the effective cloud albedo, the surface solar irradiance can be derived using the above formulas.

For the retrieval of the direct irradiance in the all sky case a formula of Mueller et al. (2009) is used, which describes the relation of the direct irradiance (all sky) SID_{allsky} to that of the clear sky direct irradiance SID_{CLS} .

$$\text{Equation 3.7: } SID_{allsky} = SID_{CLS} * (k - 0.38 \cdot (1 - k))^{2.5}$$

where k is the clear-sky index. This formula is an adaptation of the Skartveit et al. (1998) diffuse model. Here again SID_{CLS} is calculated using the MAGIC code described in section 4.4. Here only a brief outline is given.

The clear sky solar irradiance is calculated using an eigenvector look-up table method (see Mueller et al., 2009). It is based on radiative transfer modelling and enables the use of extended information about the atmospheric state. Accurate analysis of the interaction between the atmosphere, clear sky reflection, transmission and the top of atmosphere albedo has been the basis for the new method, characterized by a combination of parameterizations and "eigenvector" look-up tables. The source code of the method (Meso scale Atmospheric Global Irradiance Code – MAGIC) is available under gnu-public license at <http://sourceforge.net/projects/gnu-magic/>.

Surface solar irradiance data sets derived with the Heliosat method and the n-CAL equation (Equation 5.5) have been extensively validated against the ground-based solar radiation

 Algorithm Theoretical Basis Document Meteosat (MVIRI) Climate Data Sets of SIS, SID and CAL: MVIRI_HEL	Doc.No.: SAF/CM/DWD/ATBD/MVIRI_HEL Issue: Date: 25.01.2011
--	---

measurements (Perez et al., 2001; Wald et al., 2002; Meyer et al., 2003; Rigollier et al., 2004). It is well recognized that the surface solar irradiances derived from satellite measurements can be more accurate than that interpolated from the ground-based measurements, which are more than 30 kilometres apart (Perez et al., 1997; Zelenka et al., 1999). The validation results have demonstrated that the n-CAL relation is robust.

4 The gnu-MAGIC algorithm

4.1 Solar irradiance: Introduction and Definition

The solar surface irradiance consists of a diffuse fraction and a direct fraction. The diffuse fraction of the surface irradiance is defined as the solar radiation that has undergone scattering in the atmosphere. The direct irradiance is the flux reaching a horizontal unit of the earth's surface in the 0.2 - 4 μm wavelength band from the direction of the sun without being scattered. Both quantities are expressed in W/m^2 .

4.2 Motivation and strategy for solar surface irradiance and direct irradiance

Accurate information on the direct and total solar irradiance is important for

- + the prediction of energy yield, the planning, monitoring and system design of solar-thermal power plants (see Figure 4–1), and photovoltaic systems.
- + the analysis and understanding of the climate system.

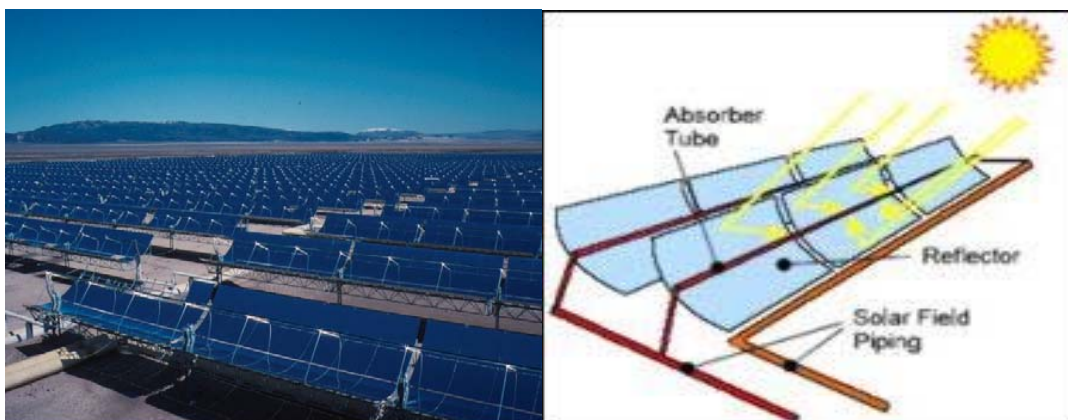


Figure 4–1: Principle of solar-thermal power plants: The concentration of solar surface irradiance enables the generation of high temperatures, hence the operation of “traditional” cost-efficient steam generators. Various prototypes have already been set up in southern Europe and Morocco.

Only few well-maintained ground measurements of direct irradiance exist in Europe, while in Africa and over the ocean almost no information on surface radiation is available from surface observations. Geostationary satellites enable the retrieval of area-wide direct irradiance in high spatial and temporal resolution with good accuracy ($<15 \text{ W/m}^2$). For solar surface irradiance a higher density of ground measurements is available in Europe. However, there exist no appropriate European network and for Africa and over the ocean the situation is almost equal to that of direct irradiance.

In the last years, CM SAF has successfully extended well-established methods used within the Solar Energy community (e.g., Skartveit et al., 1998) to include the information on the atmospheric composition nowadays available from the new generation of satellites (e.g.,

 Algorithm Theoretical Basis Document Meteosat (M VIRI) Climate Data Sets of SIS, SID and CAL: M VIRI_HEL	Doc.No.: SAF/CM/DWD/ATBD/MVIRI_HEL Issue: Date: 1.1 25.01.2011
--	---

SCIAMACHY, MSG). One important extension of the MAGIC algorithm, which is currently also used for the production of the CM SAF SIS “near-real” time product, is that it employs detailed aerosol information instead of turbidity maps. The clear sky irradiance is completely based on Radiative Transfer Modelling. Finally, the possibility to use an improved cloud mask is expected to improve the accuracy. The physical basis of the algorithm is described in Mueller et. al (2009) and R. Mueller et al. (2003).

4.3 Algorithm Overview

The retrieval of the clear sky direct irradiance and the clear sky solar surface irradiance is realised using a eigenvector look-up table (LUT) approach. For the retrieval of SIS and SID, radiative transfer model (RTM) simulations have been conducted for the irradiances and stored in LUTs (Figure 4–2).

A LUT is a data structure used to replace the time-consuming RTM computation with a simpler and faster interpolation operation within discrete pre-computed RTM results.

In order to consider the cloud effect on clear sky SIS the well established Heliosat relations is employed, see section 5 for details. For SID the approach of Skartveit et al. (1998) has been implemented, see section 6 for details. This semi-empirical approach is derived from a comparison of cloud information and ground-based measurements of global and diffuse irradiance.

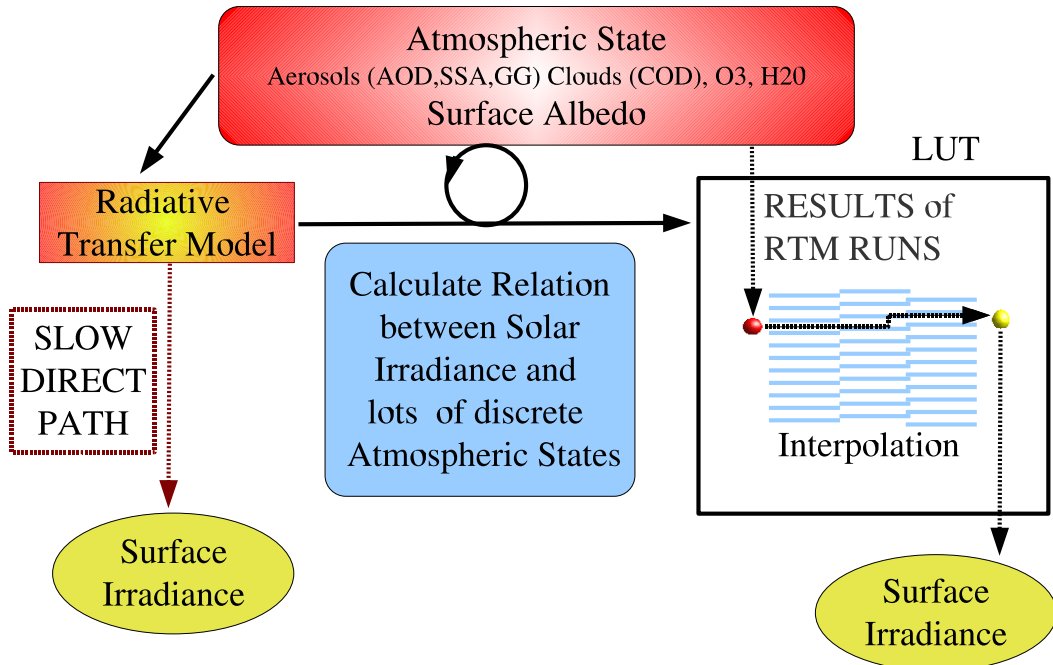


Figure 4–2: The relation of the transmission to a manifold of atmospheric states is pre-calculated with a radiative transfer model (RTM) and saved in a look-up table (LUT). Once, the LUT has been computed the transmittance for a given atmospheric state can be extracted from the LUT for each satellite pixel and time.

 Algorithm Theoretical Basis Document Meteosat (M VIRI) Climate Data Sets of SIS, SID and CAL: M VIRI_HEL	Doc.No.: SAF/CM/DWD/ATBD/MVIRI_HEL Issue: Date: 25.01.2011 1.1
--	--

4.4 The GNU-MAGIC approach for the retrieval of solar irradiance

The MAGIC approach is used to retrieve the direct irradiance SID and the solar surface irradiance SIS. It combines the hybrid-eigenvector hybrid approach for the calculation of the clear sky irradiances (both SID and SIS) with the well established Heliosat relations (see section 3.6) for the consideration of the cloud effect. The MAGIC method is described in this section while in the following sections product specific differences between the retrieval of direct and global irradiance are described and discussed in section 5 and 6 respectively.

The MAGIC code is based on the radiative transfer model calculations, following a hybrid look-up-table approach. The MAGIC code includes a basic clear-sky look-up-table (LUT), surface albedo map, water vapour climatology and aerosol climatology. The basic clear-sky LUT consists of radiative transfer model results for aerosols with different aerosol optical thickness, single scattering albedo, and asymmetry parameter. Fixed values for water vapour, ozone and surface albedo have been used for the calculation of the basis LUT: 15 kg/m² for water vapour column, 345 DU of ozone, and a surface albedo of 0.2. The effect of the solar zenith angle on the transmission, hence the surface solar irradiance, is considered by the use of the Modified Lambert Beer (MLB) function (Mueller, 2004). The effects of variations in water vapour and surface albedo relative to the fixed values used in the calculation of the basis LUT are corrected using the correction formulas and parameterizations. The databases in the MAGIC code can be updated and replaced with instantaneous measurements without changing the basic LUT and the code. Therefore the MAGIC code is fast, robust and suitable for operational algorithms.

The input parameters of the MAGIC code are date, time, solar zenith angle, latitude, longitude, effective cloud albedo (cloud index), water vapour column density, aerosol optical thickness and single scatter albedo for aerosols. The output of the MAGIC code is the clear-sky and all-sky surface solar irradiances in the 0.2-4.0 μm wavelength region. The ozone column density is a constant of 345 DU and the asymmetry parameter for the aerosol scattering phase function is also fixed at 0.7 in the current version of the MAGIC code. The extraterrestrial total solar irradiance is 1366 W/m² and adjusted according to the earth-sun distance. The n-k relation is already included in the MAGIC code. More details about the MAGIC code are described by Mueller et al. (2004, 2009)

The RTM libRadtran (Mayer and Kylling, 2005) was used for the generation of the basis LUT. RTM calculations were performed for 24 spectral bands between 250 and 3600 nm for numerous states of aerosols. Several types of aerosols were included (Hess et al., 1998). Increase in the computing performance has been achieved by the use of Modified Lambert Beer (MLB) functions (Mueller et al., 2004) and the implementation of hybrid eigenvector LUTs (Mueller et al., 2009). An extraction of relevant background information on MAGIC taken from Mueller et al (2009) is given in section 9 (Appendix A)

 Algorithm Theoretical Basis Document Meteosat (MVIRI) Climate Data Sets of SIS, SID and CAL: MVIRI_HEL	Doc.No.: SAF/CM/DWD/ATBD/MVIRI_HEL Issue: Date: 1.1 25.01.2011
--	---

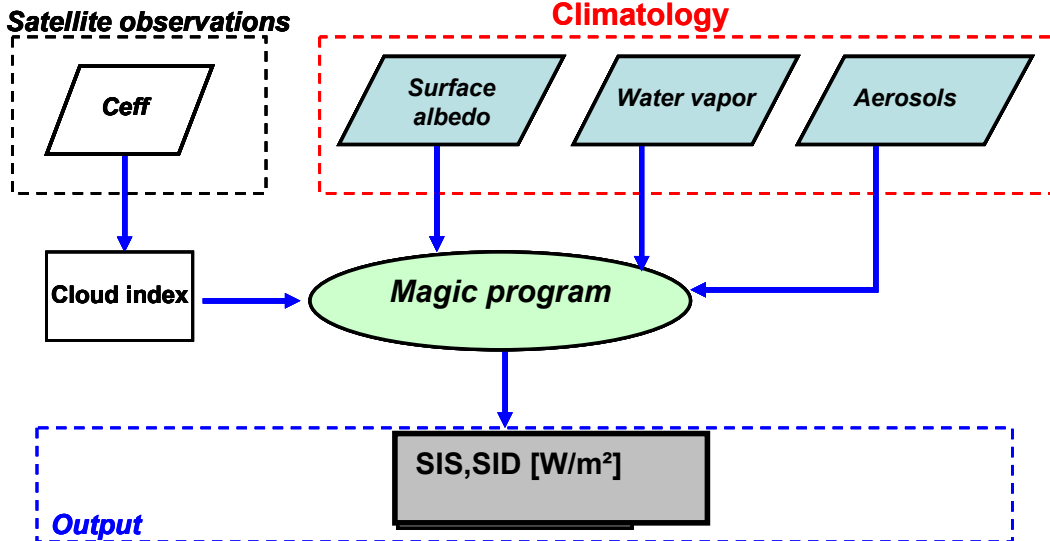


Figure 4–3: Diagram of the interface of MAGIC to the atmospheric input and the satellite observations, C_{eff} stands for the dark offset corrected and normalised Counts.

4.5 Atmospheric input information

Here the atmospheric input information used to retrieve the solar irradiance SIS and SID is described. The sensitivity of these parameters on the direct irradiance is discussed in section 6.3.

Effective cloud albedo and clear sky index:

The effective cloud albedo and clear sky index are derived with the MAGICSOL method, see section 3 for further details.

Aerosol:

Aerosols have a significant effect on the solar irradiance. They scatter and absorb solar radiation. In order to describe the effect of scattering and absorption, information about the aerosol type and aerosol optical depth is needed. The aerosol type determines the relation between scattering and absorption. This relation can be expressed in terms of the single scattering albedo. The asymmetry parameter depends also on the aerosol type (size and composition) and determines the relation between forward- and backward-scattering. However, for the calculation of direct irradiance only the aerosol optical depth is relevant, as the AOD is defined as the attenuation of direct irradiance. The aerosol type and hence the single scattering albedo and asymmetry factor are only of relevance for the total solar irradiance (diffuse + direct irradiance) and thus for the relation between direct and total solar irradiance for a given AOD (please see section 4 for details)

Monthly mean aerosol information is taken from an aerosol climatology by Kinne et al. (2005), which is based on AEROCOM (<http://dataipsl.ipsl.jussieu.fr/AEROCOM/>) model median and AERONET ground based measurements. This climatology is available in a 1x1 degree resolution and has been evaluated to perform well in Africa (Ineichen, 2010) where ground measurements are very rare.

MAGIC offers also the option to use the GADS/OPAC climatology (Hess et al., 1998, Köpke et al. 1997) with a corresponding climatological of relative humidity data by NCEP (Kalnay et

 Algorithm Theoretical Basis Document Meteosat (MVIRI) Climate Data Sets of SIS, SID and CAL: MVIRI_HEL	Doc.No.: SAF/CM/DWD/ATBD/MVIRI_HEL Issue: Date: 25.01.2011
--	---

al., 1996) to consider the effect of relative humidity on aerosol optical depth, single scattering albedo and asymmetry parameter. The aerosol climatology consists of long term monthly means either in 2.5 x 2.5 degree resolution (GADS/OPAC). However, for the generation of the climate data records, the Kinne et al. (2005) climatology has been used as this climatology has performed better for the estimation of solar irradiance than the GADS/OPAC climatology (Ineichen, 2010).

Water vapour:

Water vapour is an important absorber. It does not scatter solar radiation and its attenuation effect is pre-dominantly independent on the underlying aerosol state.

Monthly values of integrated water vapour are taken from the global reanalysis data set of ECMWF (ERA-40 and ERA-Interim). Total water vapour from the ERA-interim Reanalysis have been used from 1989 onwards. Up to 1989 ERA Reanalysis data have been used (Uppala et al., 2005 and Betts et al. 2009). Monthly means on 0.5x0.5 degree latitude-longitude grid. The pixel value is derived by spatial interpolation and assignment of the respective monthly mean.

Ozone:

Ozone is a strong absorber in the UV but the absorption is relatively weak within the broadband spectrum which is relevant for the estimation of the direct irradiance.

For ozone the climatological values from standard atmosphere are used (Krämer et al., 2003).

5 Solar surface irradiance (CM-54)

Employing the MAGIC eigenvector hybrid LUT approach the clear sky solar irradiance is calculated in a first step for the given atmospheric conditions. The atmospheric conditions cover different values for water vapour, ozone, aerosol optical depth, aerosol single scattering albedo and asymmetry parameter, and surface albedo.

Within the basic LUT the solar irradiance for the actual aerosol state is derived by linear interpolation between the pre-calculated solar irradiance values associated to different aerosol states for fixed water vapour amount of 15 mm, an ozone content of 345 DU and a surface albedo of 0.2. Deviations in water vapour, ozone and the surface albedo from the values assumed for the creation of the LUT are afterwards corrected by application of Equation 5.1 and Equation 5.2. Please see Figure 6-1 for a flow diagram of the scheme.

$$\text{Equation 5.1} \quad SIS_{COR} = SIS_{LUT} + \Delta SIS_{H2O} * \cos(SZA)^a$$

SIS_{LUT} is the solar irradiance at the surface derived from the basis LUT for fixed water vapour amount of 15mm, SIS_{COR} is the solar surface irradiance corrected for the actual (real) water vapour amount, and SZA is the solar zenith angle. ΔSIS_{H2O} is the difference between SIS for the 15 kg/m² water vapour and the real amount of water vapour, for SZA=0 and a fixed standard atmosphere defined by rural aerosol type with an AOD of 0.2, a surface albedo of 0.2 and 345 DU ozone. ΔSIS_{H2O} depends on the amount of water vapour. It is pre-calculated for 18 water vapour amounts within the range of 2.5 to 70 mm (the interpolation grid corresponds to those illustrated in Figure 5-2). The algorithm uses the appropriate ΔSIS_{H2O} value for the specific pixel and time. The exponent a is 0.88. The validity of this formula was verified by comparison with radiative transfer model results. A corresponding equation is used for the ozone correction.

 Algorithm Theoretical Basis Document Meteosat (MVIRI) Climate Data Sets of SIS, SID and CAL: MVIRI_HEL	Doc.No.: SAF/CM/DWD/ATBD/MVIRI_HEL Issue: Date: 1.1 25.01.2011
--	---

$$\text{Equation 5.2: } SIS = SIS_{COR} * (0.98 + 0.1 * SAL)$$

Equation 6.2 gives the correction of deviations in the surface albedo relative to the standard value used in the basis LUT. Here, SAL is the surface albedo and SIS_{COR} is the SIS retrieved from the LUT, but already corrected for the water vapour and ozone effect.

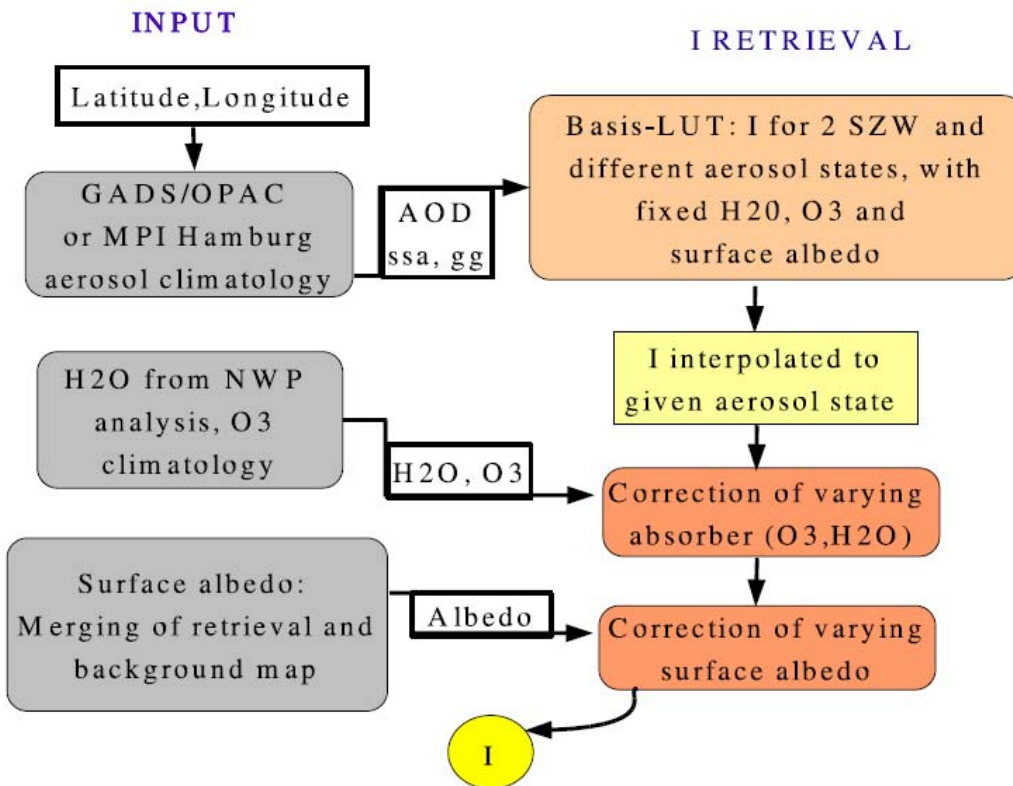


Figure 5–1: Flow-diagram of the clear sky LUT approach for SIS. NWP: Numerical Weather Prediction.

A detailed description of the hybrid-eigenvector LUT approach is given in Mueller et al. 2009, please see [gnu-magic-publex.pdf](#) for further details.

 Algorithm Theoretical Basis Document Meteosat (MVIRI) Climate Data Sets of SIS, SID and CAL: MVIRI_HEL	Doc.No.: SAF/CM/DWD/ATBD/MVIRI_HEL Issue: Date: 25.01.2011
--	---

5.1 Cloudy sky situations

The effective cloud albedo is related to the solar irradiance via the clear sky index. The clear sky index is defined as

Equation 5.3: $k = S/S / S/S_{CLS}$

Here S/S_{CLS} is the solar irradiance for cloud free skies. The relation between the effective cloud albedo CAL and the clear sky index is mainly given by:

Equation 5.4 : $k = 1 - CAL$

This relation is defined by physics, in detail by the law of energy conservation (Dagestedt, 2005). However, above a CAL value of 0.8 empirical corrections are needed in order to consider:

- ⊕ The effect of statistical noise, which could lead to CAL values above 1 and below 0 (occurs very seldom, however have to be considered).
- ⊕ The effect of saturation occurring in optical thick clouds.

In this regions the n-CAL relation was determined from the statistical regression using the ground-based measurements at European sites and fitted to get the best performance at all the ground sites. Equation 5.5 provides the complete n-CAL relation for all possible CAL values. It is important to note that the empirical fit has been performed in the 80s and used since then without refitting. The RMSD of the empirical fit is 0.1.

Equation 5.5: $CAL < -0.2, \quad k = 1.2,$
 $-0.2 \leq CAL \leq 0.8, \quad k = 1 - CAL,$
 $0.8 < CAL \leq 1.1, \quad k = 2.0667 - 3.6667 * CAL + 1.6667 * CAL^2,$
 $1.1 < CAL, \quad k = 0.05.$

As a consequence of the definition of the clear sky index, the surface solar irradiance for the full-sky situation (G) is given by,

Equation 5.6 $SIS = k * SIS_{CLS},$

Where S/S_{CLS} is the clear-sky surface solar irradiance calculated using the MAGIC code (Mueller et al., 2004, 2009), described in section 4.4.

5.2 Averaging

Daily averages are calculated following a method by Möser (1983) (also published in Diekmann et al., 1988), see Equation 5.7.

Equation 5.7: $SIS_{DA} = SIS_{CLSDA} \frac{\sum_{i=1}^n SIS_i}{\sum_{i=1}^n SIS_{CLS_i}}$

SIS_{DA} is the daily average of SIS. SIS_{CLSDA} is the daily averaged clear sky SIS, SIS_i the calculated SIS for satellite image i and SIS_{CLS_i} the corresponding calculated clear sky SIS. The number of images available during a day is denoted by n .

The larger the number of available images per day, the better the daily cycle of cloud coverage can be resolved, increasing the accuracy of the daily average of SIS. A minimum

 Algorithm Theoretical Basis Document Meteosat (MVIRI) Climate Data Sets of SIS, SID and CAL: MVIRI_HEL	Doc.No.: SAF/CM/DWD/ATBD/MVIRI_HEL Issue: Date: 1.1 25.01.2011
--	---

number of three available pixels per day is required to derive the daily mean for this specific pixel. The monthly average is calculated from the daily means of this month on pixel basis as arithmetic mean with a required number of 10 existing daily means. The hourly means are calculated as arithmetic average using Equation 3.6. The conversion from the irregular satellite projection to the regular 0.03×0.03 degree grid is done with the IDL using triangulation re-gridding (TRIGRID).

5.3 Sensitivity and dependence of atmospheric input on SIS

The sensitivity of the solar irradiance on the atmospheric input is discussed. The section provides the uncertainty or sensitivity of SIS in relation to the input parameters. The error and accuracy of SIS is assessed by comparison with in-situ data and provided within the validation report. Beside the effect of the clear sky index, aerosols and water vapour have a significant effect on the attenuation of the solar irradiance, while the surface albedo effect is rather weak.

5.3.1 Water vapour:

Figure 5–2 provides the sensitivity of the solar surface irradiance SIS on water vapour. The deviation of the direct irradiance is plotted against water vapour variations relative to 15 mm (\sim value of the USS standard atmosphere). The sensitivity depends on the solar zenith angle and the total amount of water vapour. The sensitivity is much higher for low water vapour amounts and in the order of 20 W/m^2 for variations of 5 mm water vapour, while it is below 10 W/m^2 for water vapour contents above 15 mm. The effect on the direct irradiance is only a few W/m^2 for typical water vapour uncertainties of 1-2 mm.

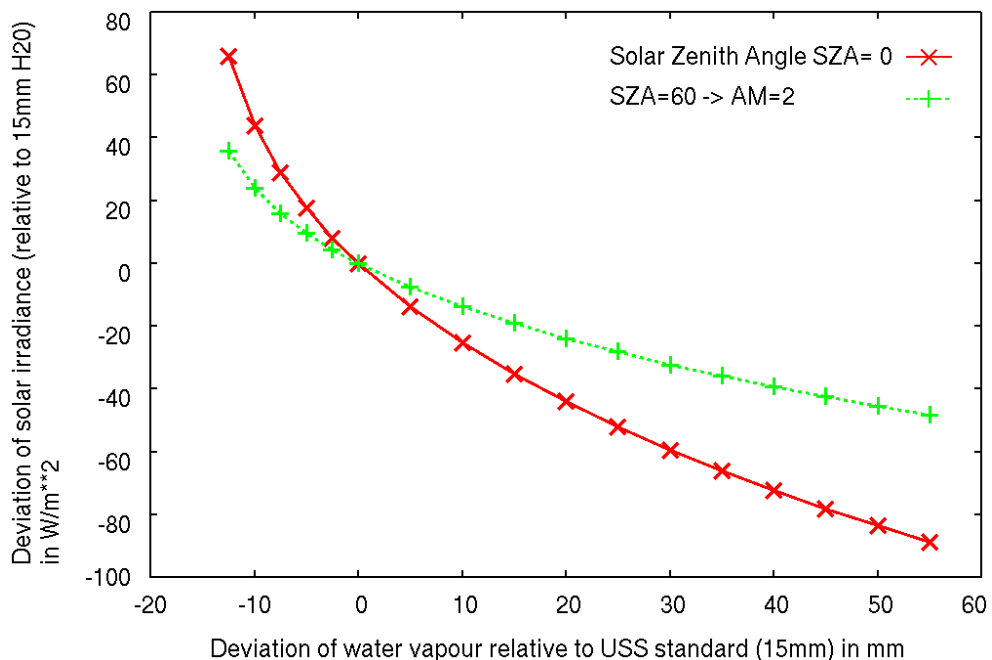


Figure 5–2: The sensitivity of solar surface SIS irradiance on water vapour variations for a SZA of 0° and 60° .

 Algorithm Theoretical Basis Document Meteosat (MVIRI) Climate Data Sets of SIS, SID and CAL: MVIRI_HEL	Doc.No.: SAF/CM/DWD/ATBD/MVIRI_HEL Issue: Date: 1.1 25.01.2011
--	---

The solar surface irradiance is slightly more sensible to uncertainties in water vapour than the direct irradiance discussed later on. The reason for this behaviour is the prolongation of the path length for solar irradiance due to multiple scattering, which is per physical definition not present in case of direct irradiance, please see Figure 5–3 for illustration of the differences.

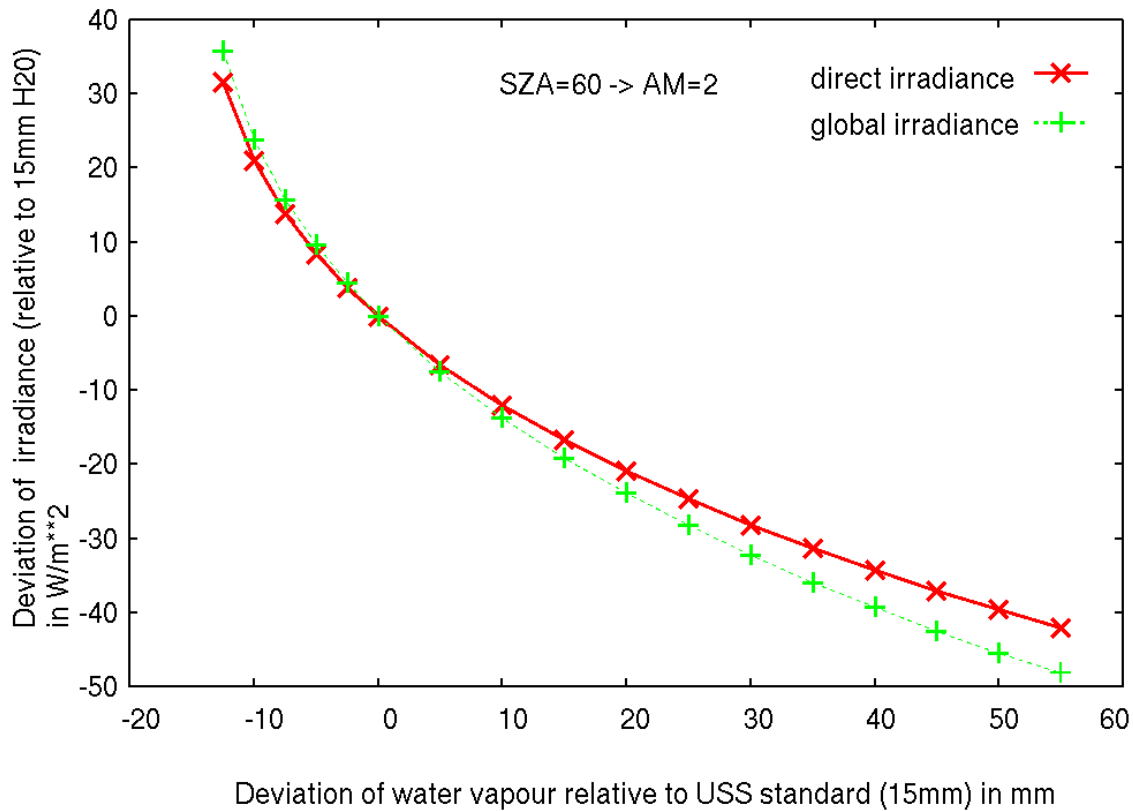


Figure 5–3: The sensitivity of “total” solar irradiance in relation to that of direct irradiance at an air mass of 2 ($SZA=60^\circ$). As can be seen the effect is not very large as both quantities show almost the same sensitivity.

5.3.2 Ozone

Figure 5–4 provides the sensitivity of the direct irradiance on ozone. The deviation of the direct irradiance is given in dependency of ozone variations relative to 345 DU (~ value of the USS standard atmosphere). The sensitivity depends on the solar zenith angle and is small throughout the ozone range. The deviation of direct irradiance is about 1 W/m^2 for typical ozone variation (+/-100 DU) within the SEVIRI disk. Again the sensitivity of the solar irradiance on ozone is slightly higher than that given for the direct irradiance.

 Algorithm Theoretical Basis Document Meteosat (MVIRI) Climate Data Sets of SIS, SID and CAL: MVIRI_HEL	Doc.No.: SAF/CM/DWD/ATBD/MVIRI_HEL Issue: Date: 1.1 25.01.2011
--	---

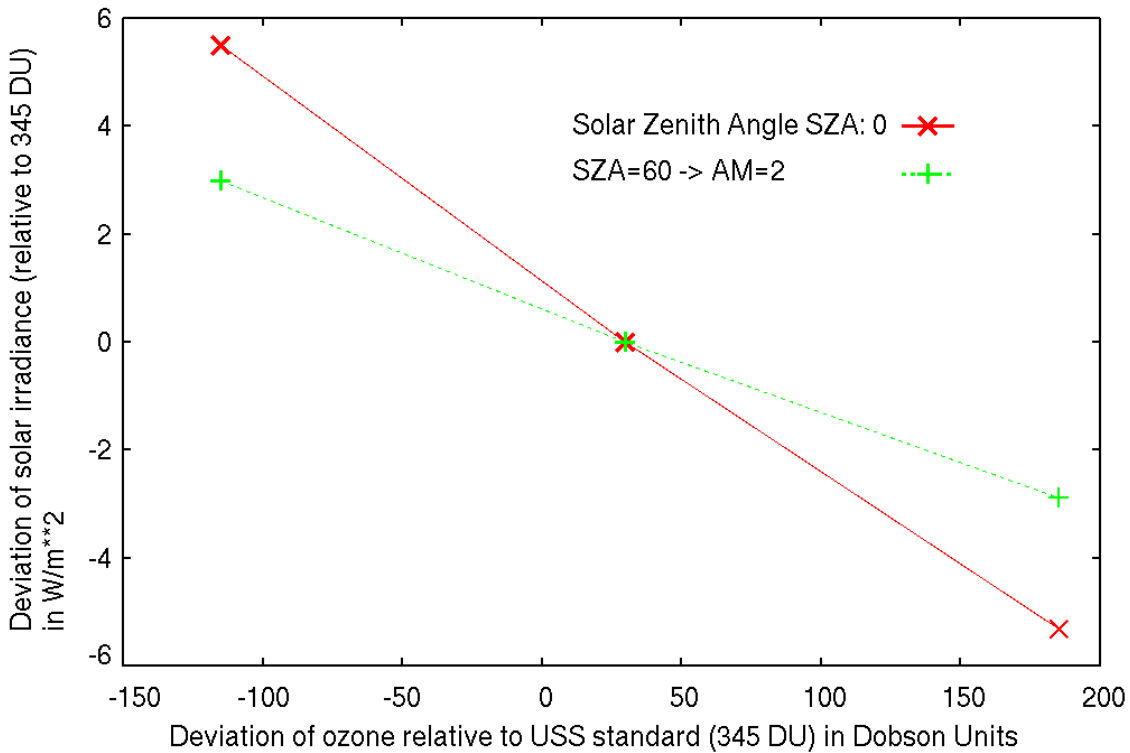


Figure 5–4: The sensitivity of solar irradiance SIS to ozone for a SZA of 0° and 60°.

5.3.3 Aerosols

Aerosol type, expressed as single scattering albedo and asymmetry parameter, has a significant effect on the solar irradiance and determines the relation between solar irradiance and direct irradiance. The single scattering albedo describes the relation between scattering and absorption, while the asymmetry parameter describes the relation between forward and backward scattering (as a consequence of the particles size). However the attenuation of the direct irradiance by aerosols is completely defined by the AOD, which by definition, describes the attenuation of the direct irradiance. Hence, for direct irradiance it is only of relevance to investigate the sensitivity on the aerosol optical depth AOD. This is depicted in Figure 5–5 and Figure 5–6. The global (total solar irradiance) and direct irradiance is plotted for the USS standard atmosphere over the aerosol optical depth for two different values of single scattering albedo for a solar zenith angle of 60 degrees and a solar zenith angle of 0 degree (Figure 5–5, Figure 5–6). The single scattering albedo has a significant effect on the global irradiance, but not on the direct irradiance, the respective RTM runs lead to identical values, see Figure 6–4 and Figure 6–5 for comparison. The effect of the AOD is much larger for the direct irradiance than for the global irradiance, hence, the sensitivity of the direct irradiance on AOD is much higher. Typical uncertainties in the monthly mean aerosol optical depth of 0.1 relative to a background of AOD=0.2 leads to uncertainties of about 10 W/m² for a solar zenith angle of 60° and about 20 W/m² for solar zenith angle of 0°.

 Algorithm Theoretical Basis Document Meteosat (MVIRI) Climate Data Sets of SIS, SID and CAL: MVIRI_HEL	Doc.No.: SAF/CM/DWD/ATBD/MVIRI_HEL Issue: Date: 1.1 25.01.2011
--	---

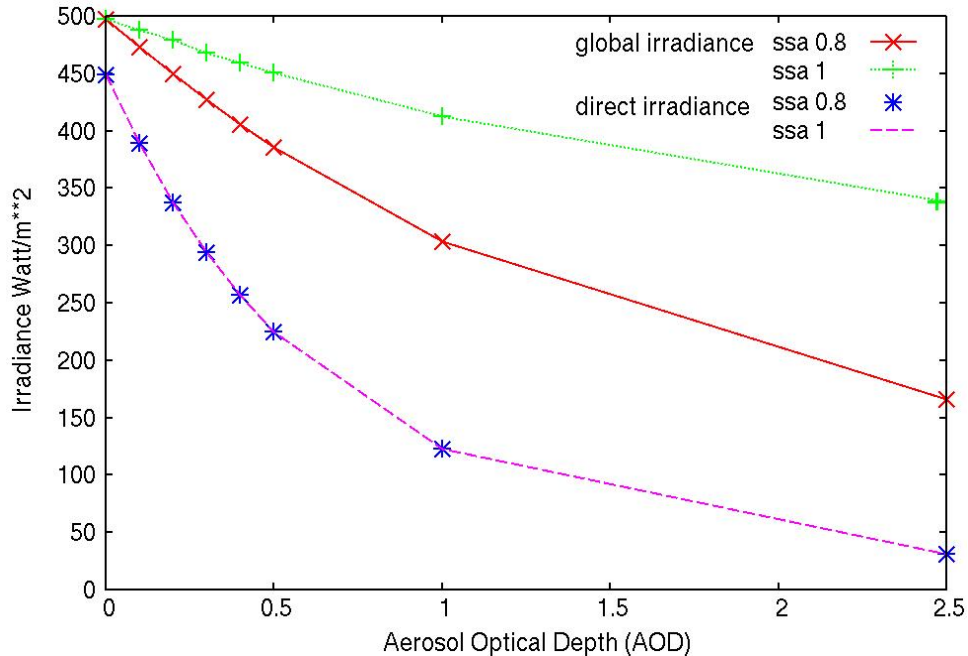


Figure 5-5: Sensitivity of Aerosol optical depth and single scattering albedo on direct irradiance in comparison to total solar irradiance for a solar zenith angle of 60° (air mass of 2).

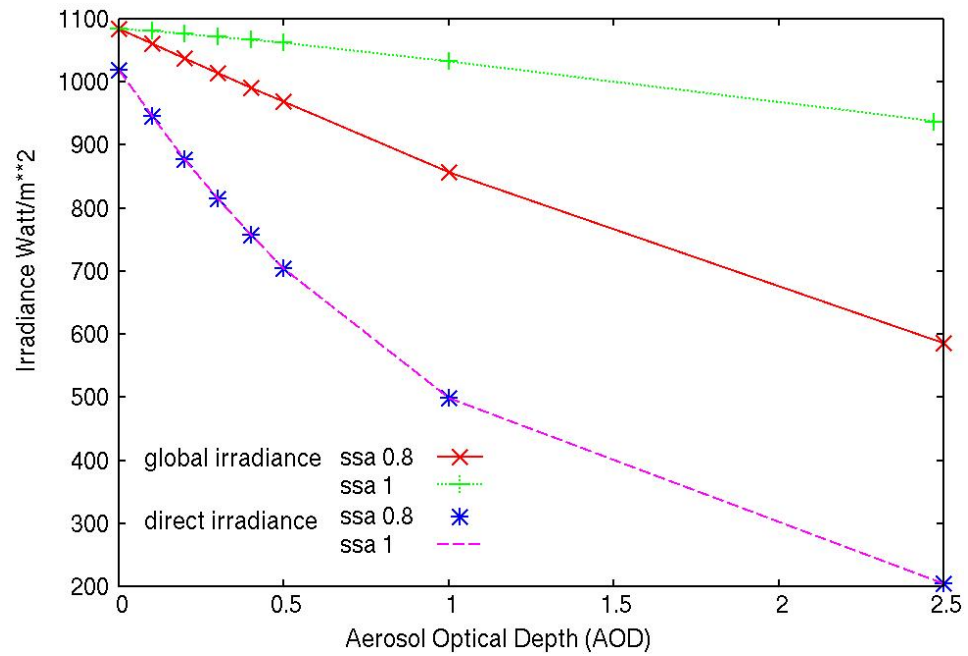


Figure 5-6: Sensitivity of Aerosol optical depth and single scattering albedo on direct irradiance in comparison to total solar irradiance for a solar zenith angle of 0°. (air mass of 2).

 Algorithm Theoretical Basis Document Meteosat (MVIRI) Climate Data Sets of SIS, SID and CAL: MVIRI_HEL	Doc.No.: SAF/CM/DWD/ATBD/MVIRI_HEL Issue: Date: 25.01.2011
--	---

5.3.4 Surface albedo

Figure 5–7 illustrates the sensitivity of clear sky SIS on uncertainties and errors in the surface albedo. Deviations of +/- 0.1 in the surface albedo lead to deviations in clear sky SIS of +/- 1%. The effect is almost linear. Errors in the surface albedo are expected to be typically less than 0.1, with exception of snow covered surfaces, where higher errors might occur. The effect is pre-dominantly independent on the clear sky atmospheric state.

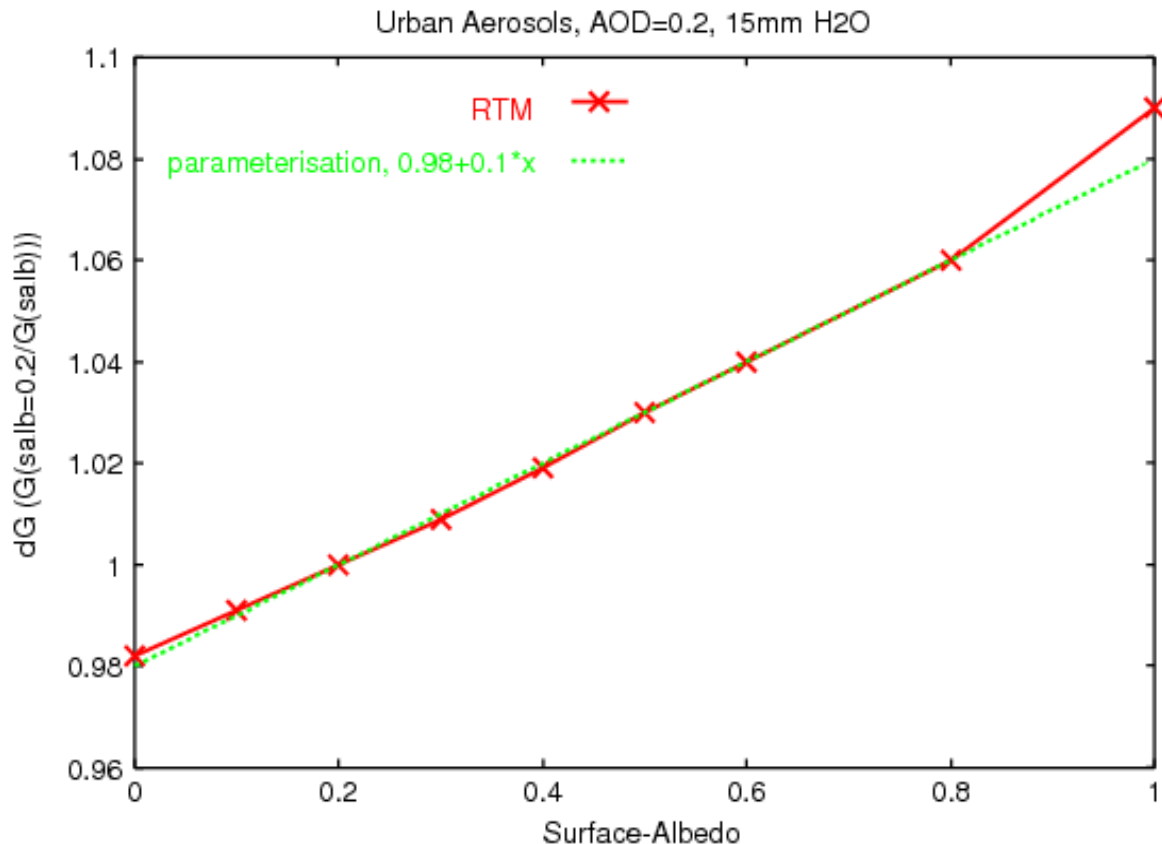


Figure 5–7: Sensitivity of the solar irradiance SIS on the surface albedo. The red line shows the RTM results and the green line the applied parameterisation. The horizontal axis shows the deviation of SIS with variable surface albedo relative to SIS calculated for a fixed surface albedo of 0.2. For deviations of +/- 0.1 in the surface albedo the uncertainty in SIS is +/- 1%. With exception of values above 0.9 the parameterisation matches the RTM results well.

5.3.5 Clear sky index

The clear sky index is calculated from the effective cloud albedo using Equation 5.5. For $CAL > 0.8$ the clouds are rather optical thick and the uncertainty in the solar irradiance is small in absolute terms. Therefore, we focus on the region between 0 and 0.8. Here any uncertainty in the effective cloud albedo leads to identical uncertainty in the clear sky index. Thus, we are only interested in the uncertainty arising from the cloud index. Therefore, we assume a perfect clear sky irradiance. As a result of the definition of the clear sky index an uncertainty of $x\%$ translates directly in the identical uncertainty in percent for the solar irradiance, meaning a 3 % uncertainty in the effective cloud albedo (=clear sky index) would lead to a 3 % uncertainty in the solar irradiance.

 Algorithm Theoretical Basis Document Meteosat (MVIRI) Climate Data Sets of SIS, SID and CAL: MVIRI_HEL	Doc.No.: SAF/CM/DWD/ATBD/MVIRI_HEL Issue: Date: 25.01.2011
--	---

5.4 Assumption, limitations and future improvements

- The high clear-sky reflection over bright surfaces (e.g., desert regions) reduces the contrast between clear-sky reflection and cloudy-sky reflection. This leads to higher uncertainties in CAL and errors in the calculation of SIS. The modified approach for the clear sky reflection improves the accuracy of SIS over bright surfaces, but the accuracy is still significantly lower than for other surfaces.
- In regions with long-lasting cloud cover the modified approach for the clear sky reflection detects snow instead. This results in an underestimation of the effective cloud albedo and errors in the solar irradiance.
- The accuracy of aerosol information is unknown in several regions of the world due to missing ground measurements. Any uncertainty in the aerosol information affects the accuracy of SIS, especially in regions that are dominated by cloudless sky.
- **For the calculation of the look-up tables of the clear sky model standard ozone and aerosol profiles are used. These profiles are scaled with the respective vertical column values, see Mayer and Kyling (2005) for further details.,**
- **The USS standard atmosphere has been used to consider the effect of air molecules (e.g. Rayleigh scattering). However, this has no effect on accuracy (Mueller et al, 2009)**

The performed validation indicates that the accuracy of the SIS monthly and daily mean product is better than 10 W/m² and 15 W/m², respectively, which is a very promising result. Details of the validation results are given in the validation report [RD.2]

6 Direct irradiance (CM-106)

The MAGIC eigenvector hybrid LUT approach is used for the calculation of the clear sky direct irradiance for given atmospheric conditions. The atmospheric conditions cover different values for water vapour, ozone, aerosol optical depth, aerosol single scattering albedo and asymmetry parameter.

The forward scattering is considered but only from the direction of the sun, assuming the sun as a point source. Any forward scattering from the sun corona is not considered.

Within the basic LUT the direct irradiance for the actual aerosol state is derived by linear interpolation between the pre-calculated direct irradiance values associated to different aerosol states for a fixed water vapour amount of 15 mm and an ozone content of 345 DU. Deviations in water vapour and ozone are afterwards corrected by application of Equation 5.1, with SID instead of SIS and a value of 1 for the exponent a. The process flow is similar to that of SIS, as illustrated in Figure 6–1, with the exception that the surface albedo is not considered for the direct irradiance.

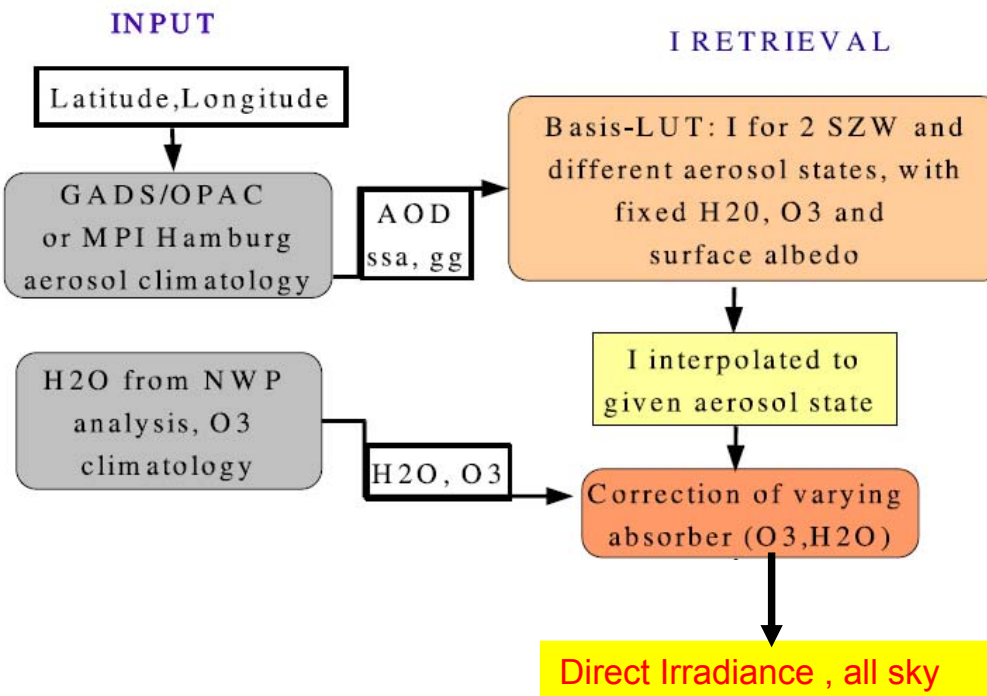


Figure 6–1: Flow-diagram of the clear sky LUT approach. NWP: Numerical Weather Prediction.

A detailed description of the hybrid-eigenvector LUT approach is given in Mueller et al. 2009.

 Algorithm Theoretical Basis Document Meteosat (MVIRI) Climate Data Sets of SIS, SID and CAL: MVIRI_HEL	Doc.No.: SAF/CM/DWD/ATBD/MVIRI_HEL Issue: Date: 1.1 25.01.2011
--	---

The effect of clouds is considered by an Equation 6.1 of Mueller et al. 2009 which was in turn developed based on the work of Skartveith et al. (1998)

$$\text{Equation 6.1: } SID_{\text{allsky}} = SID_{\text{clear}} * (k - 0.38 \cdot (1 - k))^{2.5}$$

The equation describes the relation of the direct irradiance (all sky) SID_{allsky} to that of the clear sky direct irradiance SID_{clear} . Above a CAL value of 0.6 the direct irradiance is getting zero according to Equation 6.1, which is in line with observations (Skartveith et al. (1998), Mueller et al. (2003-b)). Thereby, k is the clear-sky index. The clear sky index k is the ratio between the solar surface irradiance for all sky and for clear sky. The clear sky irradiance is derived with gnu-MAGIC, see section 4.4

6.1 Averaging

6.2 Averaging

Daily averages are calculated following a method by Möser (1983) (also published in Diekmann et al., 1988), see Equation 5.7.

$$\text{Equation 6.2: } SID_{DA} = SID_{CLSDA} \frac{\sum_{i=1}^n SID_i}{\sum_{i=1}^n SID_{CLS_i}}$$

SID_{DA} is the daily average of SID. SID_{CLSDA} is the daily averaged clear sky SID, SID_i the calculated SID for satellite image i and SID_{CLS_i} the corresponding calculated clear sky SID.

The number of images available during a day is denoted by n .

The larger the number of available images per day, the better the daily cycle of cloud coverage can be resolved, increasing the accuracy of the daily average of SID. A minimum number of three available pixels per day is required to derive the daily mean for this specific pixel. The monthly average is calculated from the daily means of this month on pixel basis as arithmetic mean with a required number of 10 existing daily means. The hourly means are calculated as arithmetic average using Equation 3.6. The conversion from the irregular satellite projection to the regular 0.03x0.03 degree grid is done with the IDL using triangulation regridding (TRIGRID).

6.3 Sensitivity and dependence of atmospheric input on direct irradiance

The sensitivity of the direct irradiance on the atmospheric input is discussed. This section provides the uncertainty or sensitivity of the direct irradiance in relation to the input parameter. The error and accuracy of SID is assessed by comparison with in-situ data and provided within the validation report. Beside the effect of the clear sky index, aerosols and water vapour have a significant effect on the attenuation of the direct irradiance.

6.3.1 Water vapour:

Figure 6-2 provides the sensitivity of the direct irradiance on water vapour. The deviation of the direct irradiance is plotted against water vapour variations relative to 15 mm (~ value of

 Algorithm Theoretical Basis Document Meteosat (MVIRI) Climate Data Sets of SIS, SID and CAL: MVIRI_HEL	Doc.No.: SAF/CM/DWD/ATBD/MVIRI_HEL Issue: Date: 1.1 25.01.2011
--	---

the USS standard atmosphere). The sensitivity depends on the solar zenith angle and the total amount of water vapour. The sensitivity is much higher for low water vapour amounts and in the order of 20 W/m^2 for variations of 5 mm water vapour, while it is below 10 W/m^2 for water vapour contents above 15 mm. The effect on the direct irradiance is only a few W/m^2 for typical water vapour uncertainties of 1-2 mm.

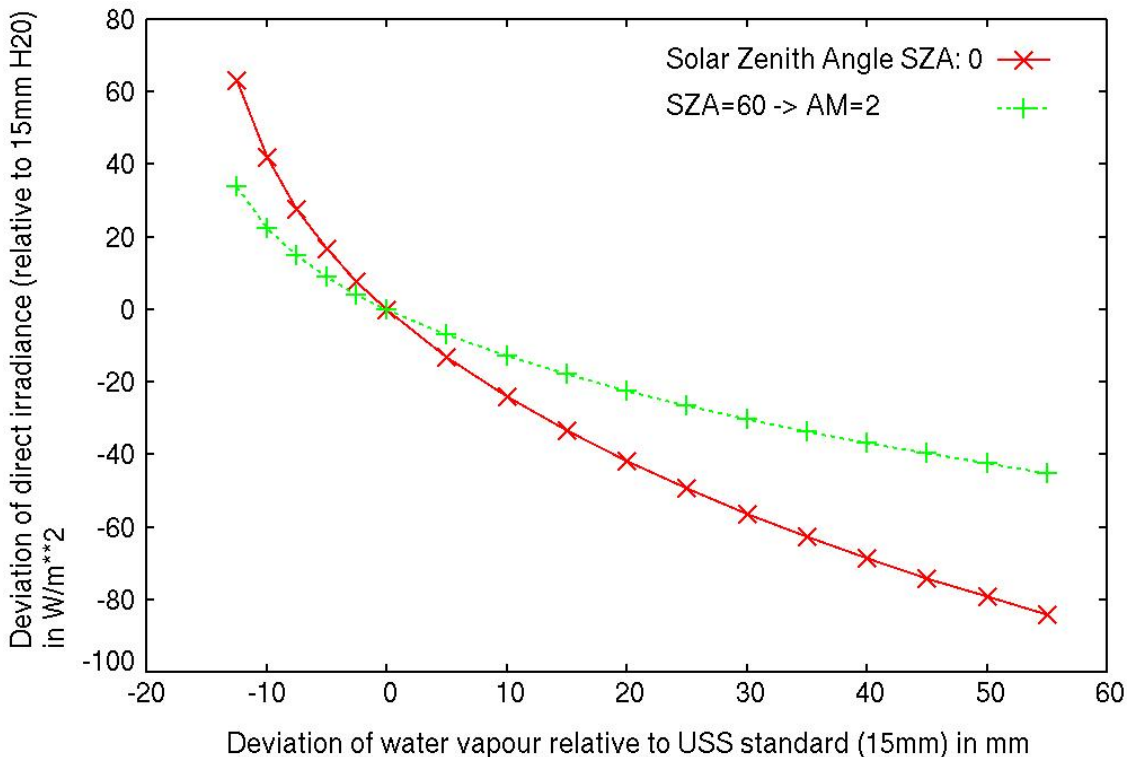


Figure 6-2: The sensitivity of direct irradiance on water vapour for a SZA of zero and 60 degree.

6.3.2 Ozone

Figure 6-3 provides the sensitivity of the direct irradiance on ozone. The deviation of the direct irradiance is given in dependency of ozone variations relative to 345 DU (~ value of the USS standard atmosphere). The sensitivity depends on the solar zenith angle and is small throughout the ozone range. The deviation of direct irradiance is about 1 W/m^2 for typical ozone variation (+/-100 DU) within the SEVIRI disk.

 Algorithm Theoretical Basis Document Meteosat (MVIRI) Climate Data Sets of SIS, SID and CAL: MVIRI_HEL	Doc.No.: SAF/CM/DWD/ATBD/MVIRI_HEL Issue: Date: 1.1 25.01.2011
--	---

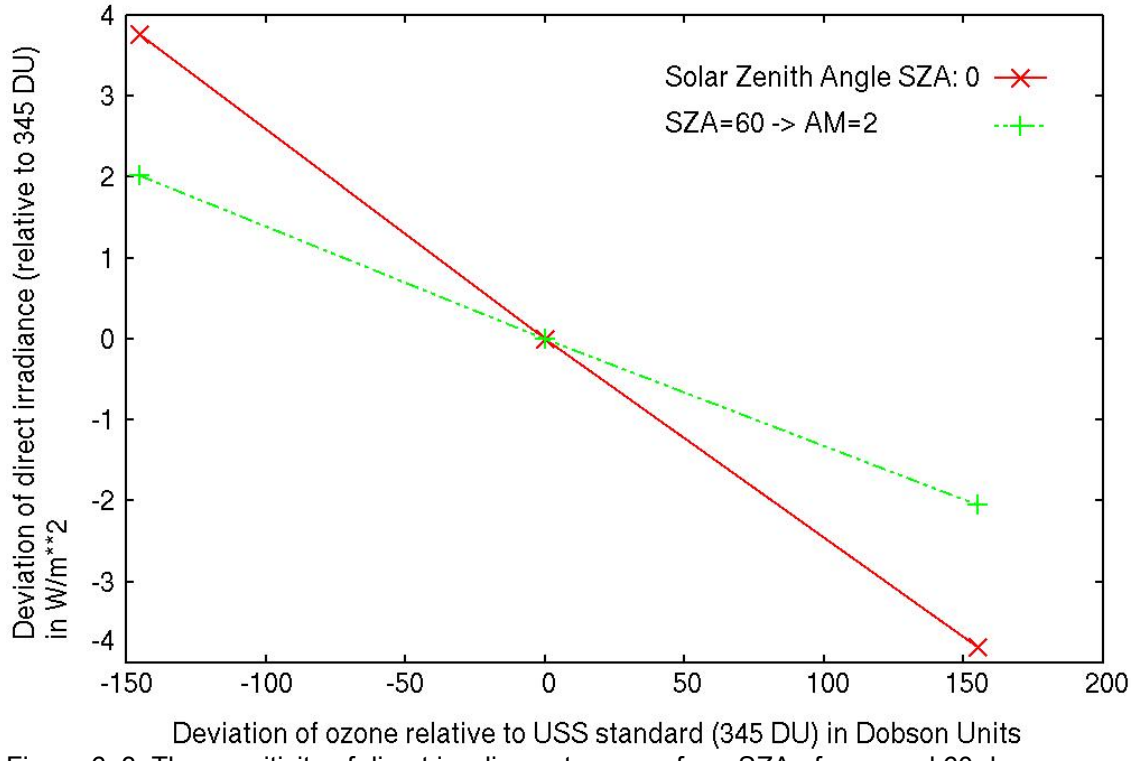


Figure 6-3: The sensitivity of direct irradiance to ozone for a SZA of zero and 60 degree.

6.3.3 Aerosols

Aerosol type, expressed as single scattering albedo and asymmetry parameter, has a significant effect on the solar irradiance and determines the relation between solar irradiance and direct irradiance. However the attenuation of the direct irradiance by aerosols is defined by the AOD, which by definition, describes the attenuation of the direct irradiance. Hence, for direct irradiance it is only of relevance to investigate the sensitivity on the aerosol optical depth AOD. This is depicted in Figure 6-4 and Figure 6-5. The global (total solar irradiance) and direct irradiance is plotted for the USS standard atmosphere over the aerosol optical depth for two different values of single scattering albedo for a solar zenith angle of 60 degrees and a solar zenith angle of 0 degree (Figure 6-4 and Figure 6-5). The single scattering albedo has a significant effect on the global irradiance, but not on the direct irradiance, the respective RTM runs lead identical values, see Figure 6-4 and Figure 6-5. The effect of the AOD is much larger for the direct irradiance than for the global irradiance, hence, the sensitivity of the direct irradiance on AOD is much higher. Typical uncertainties in the monthly mean aerosol optical depth of 0.1 relative to a background of AOD=0.2 leads to uncertainties of about 10 W/m² for AM2 and about 20 W/m² for solar zenith angle of 0 degree.

 Algorithm Theoretical Basis Document Meteosat (MVIRI) Climate Data Sets of SIS, SID and CAL: MVIRI_HEL	Doc.No.: SAF/CM/DWD/ATBD/MVIRI_HEL Issue: Date: 1.1 25.01.2011
--	---

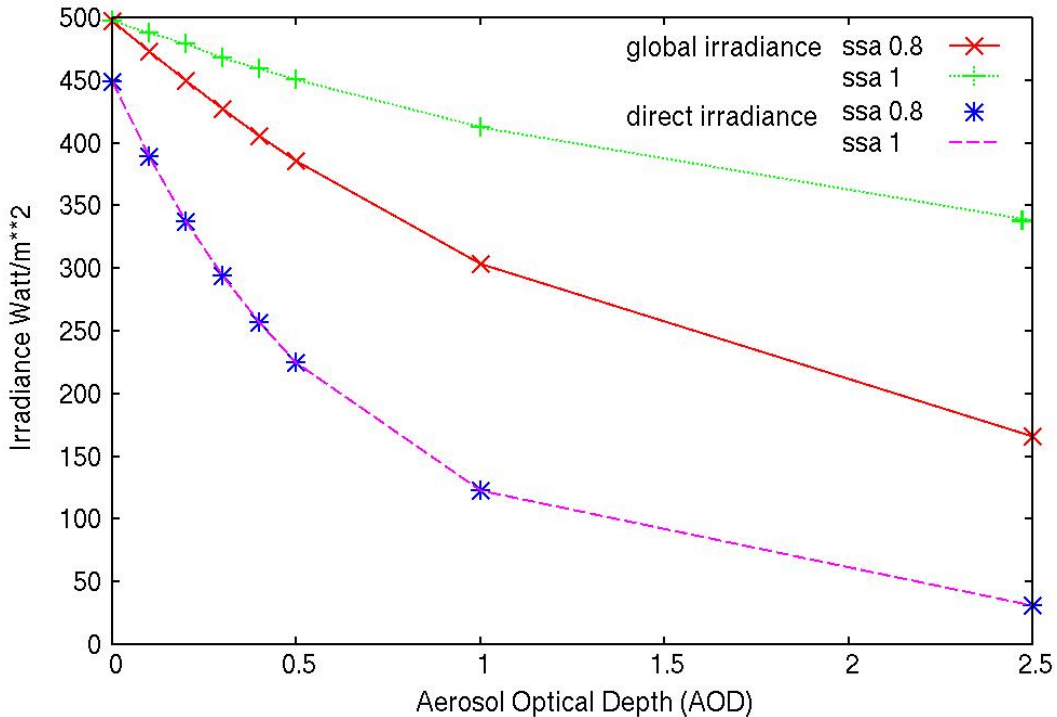


Figure 6–4: Sensitivity of Aerosol optical depth and single scattering albedo on direct irradiance in comparison to total solar irradiance for a solar zenith angle of 60 degree (air mass of 2)

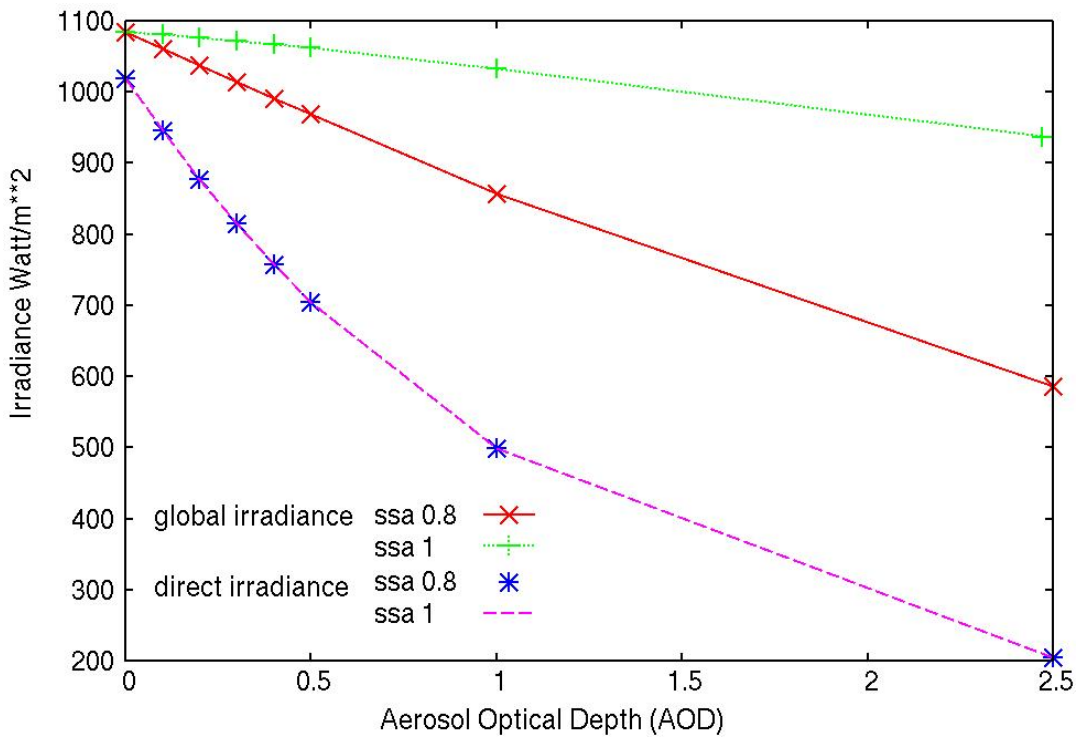


Figure 6–5: Sensitivity of Aerosol optical depth and single scattering albedo on direct irradiance in comparison to total solar irradiance for a solar zenith angle of 0 degree.

 Algorithm Theoretical Basis Document Meteosat (MVIRI) Climate Data Sets of SIS, SID and CAL: MVIRI_HEL	Doc.No.: SAF/CM/DWD/ATBD/MVIRI_HEL Issue: Date: 25.01.2011 1.1
--	--

6.3.4 Clear sky index

The clear sky index is derived from the CM SAF SIS product and is used to consider the effect of clouds on the clear sky irradiance, using equation 1. The dependence of the direct irradiance on the clear sky index is shown in Figure 6–6, together with the deviation of the direct irradiance resulting from the uncertainty of the clear sky index.

It is evident that the dependency / sensitivity of the direct irradiance on the clear sky index is comparable large. An uncertainty of 2% has been evaluated for the clear sky index based on the accuracy of the SIS CM SAF product and the sensitivity of the clear sky index on uncertainties in ρ_{\max} (section 3.4). This uncertainty leads to deviations of about 10 % in the direct irradiance, demonstrating the importance of an accurate clear sky index (hence SIS) on the direct irradiance.

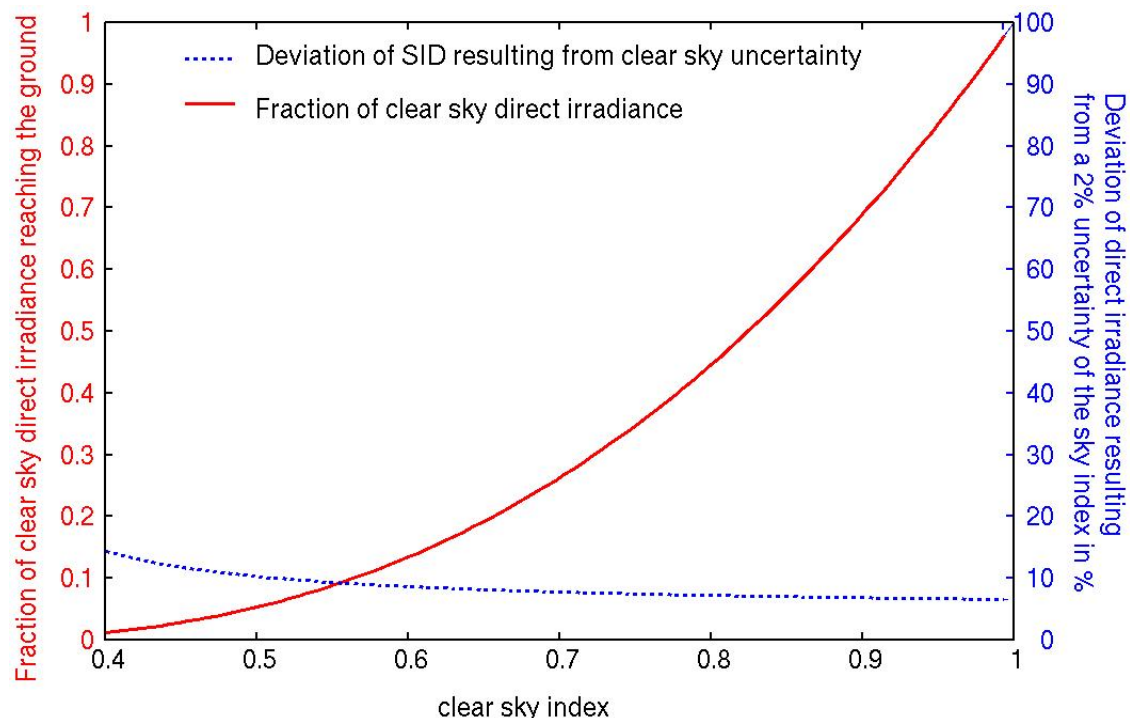


Figure 6–6: Sensitivity of direct irradiance on the clear sky index.

6.4 Assumption, limitations and future improvements

The quality of the direct irradiance strongly depends on the quality of the information about the atmospheric state, especially the aerosol information, the integrated water vapour and the clear sky index.

Accounting for the spatial variability of clouds in Equation 5.6 has the potential to improve the accuracy of the product. This could be achieved by empirical adjustment of Equation 5.6 using the spatial variance of a 15x15 km domain as measure for the spatial variability (in homogeneity) of clouds.

The limitations in SIS arising from the clear sky index discussed in section 5.4 hold also for SID, but SID is much more sensible to errors in the clear sky index.

 Algorithm Theoretical Basis Document Meteosat (MVIRI) Climate Data Sets of SIS, SID and CAL: MVIRI_HEL	Doc.No.: SAF/CM/DWD/ATBD/MVIRI_HEL Issue: Date: 1.1 25.01.2011
--	---

The higher sensitivity of SID on the aerosol optical depth and the clear sky index explains the lower accuracy of SID relative to SIS. However, the performed validation demonstrates that the accuracy of the SID monthly mean product meet the target accuracy of 15 W/m², which is a very promising result. Details of the validation results are given in the validation report [RD.2]. It is important to note that limitations in the atmospheric input are not limitations of the algorithm or method applied.

7 References

- Betts A. K., M. Köhler and Y. Zhang, 2009: Comparison of river basin hydrometeorology in ERA-Interim and ERA-40 reanalyses with observations, *Journal of Geophysical Research*, **114**, D02101, doi: 10.1029/2008JD010761
- Beyer, H. G., Costanzo, C., and Heinemann, D., 1996: Modifications of the heliosat procedure for irradiance estimates from satellite images, *Solar Energy*, **56**, 207-212.
- Cano, D., Monget, J. M., Albuisson, M., Guillard, H., Regas, N., and Wald, L., 1986: A method for the determination of the global solar-radiation from meteorological satellite data, *Solar Energy*, **37**, 31-39.
- Dagestad, K.-F. (2004), Mean bias deviation of the Heliosat algorithm for varying cloud properties and sun-ground-satellite geometry, *Theor. Appl. Climatol.*, **79**, 215–224, DOI 10.1007/s00704-004-0072-5
- Dagestad K.-F., J. A. Olseth, 2007: A modified algorithm for calculating the cloud index, *Solar Energy*, **81**, 280–289.
- Derrien,M., LeGLEAU, H., 2005: MSG/SEVIRI cloud mask and type from SAFNWC. *Int. J. Rem. Sens.*, **26**, 4707 – 4732.
- Duerr, B., and Zelenka, A., 2009: Deriving surface global irradiance over the alpine region from meteosat second generation data by supplementing the heliosat method, *Int. J. Rem. Sens.*, **30**, 5821-5841, DOI 10.1080/01431160902744829.
- Hammer, A., Heinemann, D., Hoyer, C., Kuhlemann, R., Lorenz, E., Mueller, R., and Beyer, H. G., 2003: Solar energy assessment using remote sensing technologies, *Remote Sens. Environ.*, **86**, 423–432.
- Hess, M.; P. Köpke; I. Schult, 1998: Optical Properties of Aerosols and Clouds: The Software Package OPAC. *Bull. Amer. Meteor. Soc.*, **79**, 831-844.
- Kinne, S., M. Schulz, C. Textor et al., 2006, an AEROCOM initial assessment – optical properties in aerosol component modules of global models, *Atmos. Chem. Phys.*, **6**, 1815-1834.
- Krämer, M., Ri. Mueller, H. Bovensmann, J.Burrows, J.-U. Grooß, D. S. McKenna, Ro. Mueller, Th. Woyke, J. Brinkmann, E.P. Röth, R. Ruhnke, G. Guenther, J. Hendricks, E. Lippert, K. S. Carslaw, Th. Peter, A. Zieger, Ch. Bruehl, B. Steil and R. Lehmann, 2003: Intercomparison of Numerical Stratospheric Chemistry Models under Polar Vortex Conditions. *J. of Atmospheric Chemistry*, **45**, 51-77.
- Ineichen, P., 2010: Satellite based short wave irradiance validation over Africa“, Visiting Scientist report of CM SAF, available at <http://www.cmsaf.eu>.
- Köpke, P.; Hess, M.; Schult, I.; Shettle, E., 1997: Global aerosol data set. Tech. Rep., 243, MPI Meteorology, Hamburg.

 Algorithm Theoretical Basis Document Meteosat (M VIRI) Climate Data Sets of SIS, SID and CAL: M VIRI_ HEL	Doc.No.: SAF/CM/DWD/ATBD/MVIRI_HEL Issue: Date: 1.1 25.01.2011
---	---

- Mayer, B.; A. Kylling, 2005: Technical note: "The libRadtran software package for radiative transfer calculations - description and examples of use." *Atmos. Chem. Phys.*, **5**, 1855-1877.
- Majewski, D., Liermann, D., Prohl, P., Ritter, B., Buchhold, M., Hanisch, T., Paul, G. Wergen, W. Baumgardner, J., 2002. The Operational Global Icosahedral-Hexagonal Gridpoint Model GME: Description and High-Resolution Tests, *Mon. Wea. Rev.*, **130**, 319-330.
- Möser, W. , 1983: Globalstrahlung aus Satellitenmessungen. Mitteilungen aus dem Institut für Geophysik und Meteorologie der Universität zu Köln, 37, Köln.
- Mueller, R.W.; Dagestad, K.F.; Ineichen, P.; Schroedter-Homscheidt, M.; Cros, S. Dumortier, D.; Kuhlemann, R. ; Olseth, J.A.; Piernavieja, G.; Reise, C.; Wald, L.; Heinemann,D.; 2004: "Rethinking satellite based solar irradiance modelling – The SOLIS clear sky module", *Rem. Sens. Environ.*, **91**, 160-174.
- Mueller, R.W. et al., 2003-b „Report of the HELIOSAT-3 software package for solar irradiance retrieval, all sky working version“ EU report of the Heliosat-3 project (www.heliosat3.de), NNE5-2000-00413
- Mueller, R.W., Matsoukas, C. Behr, H.D., Gratzki, A. Hollmann, R., 2009: MAGIC - The CM SAF operational scheme for the satellite based retrieval of solar surface irradiance - a LUT based eigenvector hybrid approach. *Rem. Sens. Environ.*, **113**, 1012-1024.
- Posselt R. , Mueller R. W., Stöckli R., Trentmann, J., 2011: Self calibration across Meteosat first and second generations, (submitted to Remote Sensing: Special Issue "Remote Sensing in Climate Monitoring and Analysis").
- Rigollier, C., Lefevre, M., Blanc, P., and Wald, L., 2002: The operational calibration of images taken in the visible channel of the meteosat series of satellites, *J. Atmos. Ocean. Technol.*, **19**, 1285-1293.
- Schulz, J., P. Albert, H.-D. Behr, D. Capron, H. Deneke, S. Dewitte, B. Dürr, P. Fuchs, A. Gratzki, P. Hechler, R. Hollmann, S. Johnston, K.-G. Karlsson, T. Manninen, R. Müller, M. Reuter, A. Riihelä, R. Roebeling, N. Selbach, A. Tetzlaff, W. Thomas, M. Werscheck, E. Wolters, and A. Zelenka, 2009: Operational climate monitoring from space: the EUMETSAT satellite application facility on climate monitoring (CM SAF). *Atmospheric Chemistry and Physics*, **9**, 1–23.
- Skartveit, A., Olseth, J., Tuft, M., 1998: An hourly diffuse fraction model with correction for variability and surface albedo. *Solar Energy*, **63**, 173–183.
- Uppala, S., P. Kallberg, A. Simmons, U. Andrae, V. Da Costa Bechtold, M. Firino, J. Gibson, J. Haseler, A. Hernandez, G. Kelly, X. Li, K. Onogi, S. Saarinen, N. Sokka, R. Allan, E. Andersson, E. Arpe, M. Balmaseda, A. Beljaars, Van De L. Berg, J. Bidlot, N. Bormann, S. Caires, F. Chevallier, A. Dethof, M. Dragosavac, M. Fisher, M. Fuentes, S. Hagemann, E. Holm, B. Hoskins, L. Isaksen, P. Janssen, R. Jenne, A. McNally, J.-F. Mahfouf, J.-J. Morcrette, N. Rayner, R. Saunders, P. Simon, A. Sterl, K. Trenberth, A. Untch, D. Vasiljevic, P. Viterbos and J. Woollen, 2005: The ERA-40 reanalysis. , *Q. J. R. Met. Soc.*, **131**, 2961 – 3012.
- Zelenka, A., 2001: Estimating insolation over snow covered mountains with meteosat vis-channel: A time series approach, Proceedings of the EUMETSAT Meteorological Satellite Data Users Conference, EUMETSAT Publ. EUM P, 346–352,

 Algorithm Theoretical Basis Document Meteosat (MVIRI) Climate Data Sets of SIS, SID and CAL: MVIRI_HEL	Doc.No.: SAF/CM/DWD/ATBD/MVIRI_HEL Issue: Date: 1.1 25.01.2011
--	---

8 Glossary

AVHRR:	Advanced Very High Resolution Radiometer
AOD:	Aerosol Optical Depth
CAL:	Effective cloud albedo
COT	Cloud optical depth
GADS/OPAC:	Global Aerosol Data Set / Optical Properties of Aerosols and Clouds
GERB:	Geostationary Earth Radiation Experiment
K:	Clear sky index.
LUT:	Look-up table
MVIRI:	Meteosat Visible-InfraRed Imager
NOAA:	National Oceanic and Atmospheric Administration
NCEP:	National Center for Environmental Prediction
RTM:	Radiative Transfer Model
SID:	Surface Direct Irradiance (beam).
SIS:	Solar Surface Irradiance
SZA:	Sun Zenith Angle
SSA:	Single Scattering Albedo

9 Appendix A: gnu-MAGIC documentation containing further algorithm information of gnu-MAGIC